Report on Sabbatical activities for the 2024-2025 Academic Year.

Dr. Derek D. Wright, School of Chemistry, Environmental, and Geosciences.

Summary: My sabbatical leave for the 2024-25 academic year was focused on research related to development of analytical techniques and applications for microscopy and microanalysis, specifically our JEOL JSM IT200LA Scanning Electron Microscope with an Energy Dispersive x-ray Spectrometer (SEM-EDS), Bruker M4 Tornado Plus micro X-Ray Fluorescence spectrometer (μXRF), and Agilent 8700 Laser Direct Infra-Red (LDIR) chemical imaging system. I also continued efforts focused on applications of atomic spectroscopy, environmental chemistry, and wastewater epidemiology. These efforts were successful and resulted in 3 publications and 14 conference presentations. Additionally, I completed a one-week training course in micro X-Ray Fluorescence spectroscopy in Madison WI, which significantly improved my expertise and will benefit my course instruction. I also engaged in a number out outreach activities including electron microscopy activities for visiting groups and prospective students.

Research Objectives:

The research objectives for my sabbatical were as follows

1. **Develop and apply μXRF and SEM-EDS chemical Imaging and microanalysis methods for the following research applications:**
    - **Biological Tissues** – Methods were developed for imaging nutrient and potentially toxic elements in plants, fungi, worms, and zebrafish. Results from these newly implemented methods were key to achieving my research goals and can be found disseminated in items b, e, f, l, and o (see list below). Major finding include new insights on lead bioaccumulation by plants located in shooting ranges which suggest active transport to leaf margins and damaged tissue as well as mechanistic controls on copper uptake from sites of natural copper enrichment.
    - **Geologic and Environmental Samples** Elemental imaging was crucial to geochemical interpretation of rocks, minerals, and soils in items d-j, l, m, o, and p (see below). Micro XRF additionally has allowed us to utilize Laue diffraction mapping to elucidate crystal grain structure, improving interpretation of material

phases. Further improvements are now enabled by our newly developed x-ray backscatter imaging using µXRF, which our group is the first to our knowledge to systematically apply to geological specimens. We are currently drafting a manuscript describing these findings for publication in early 2026.

- **Engineered Materials & Archeological Specimens.** We have applied elemental imaging and x-ray backscatter imaging to better understand the historical use of heavy metal based pigments in books, and to solve practical engineering problems such as sources heavy metal contamination from vape cartridges and respective failure modes. As part of this work, we inadvertently discovered that some polymer (plastic) vape cartridges appear to leach (partially dissolve) into vape fluids, which could have significant implications for product safety. As highlighted in the December 2025 Academic Affairs Report, Alex Eckman (Cannabis Chemistry) was awarded an ElSohly Award for his part in this work, presented by the Cannabis Chemistry Subdivision of the American Chemical Society, which recognizes outstanding contributions to advancing the field of cannabis and cannabinoid science. His work titled "Evidence of Pre-Use Polymer Leaching in Hemp-Derived Vaporizers" presented critical findings on material stability and safety in hemp vaporizer hardware, identifying pre-use polymer leaching and emphasizing the need for enhanced quality control in product manufacturing.

2. **Develop correlative imaging approaches using a combination of SEM-EDS, µXRF, and LDIR imaging as a novel tool to correlate element and mineral distributions in geologic samples for studies in mineralogy, petrology, and paleoclimate.**
    - **Mineralogy and Petrology** – We have made significant progress in this research area which has been presented in items h, j, and m. This work may also be featured in an upcoming publication from Agilent Technologies pending approval of the use of our data. A manuscript detailing this work, potentially the first in the world, is under development for 2026.
    - **Paleoclimate** – We have made significant progress in this research area which has been presented in items i and m, and actively continue work in this area.

3. **Metal Bioaccumulation and Metal Tolerance Mechanisms in Metal Enriched Soil and Potential Identification of Novel Hyperaccumulators.**
    - We continue to work at two interesting field sites, the Freda Stamp Mill west of Houghton MI and the Gaines Highway Shooting Area north of Kinross MI. Results from work at these sites is described in items e, f, g, l, and o.

Freda Stamp Mill Site on the Lake Superior shore west of Houghton MI.

Gaines Hwy. Shooting Area north of Kinross MI

4. **Potentially Toxic Metals in Cannabis Rolling Papers**
    - We continue work on a follow up to our April 2024 publication Elemental Composition of Commercially Available Cannabis Rolling Papers (*ACS Omega*). We have since documented the use of previously undocumented Mo and Cr based pigments and have tentatively identified common copper based pigments including copper phthalocyanine.

Additional Research Activities: In addition to the above activities, I also continued my ongoing research on wastewater epidemiology resulting in a publication comparing variant testing kits and whole genome sequencing for SARS COV-2 variant detection in wastewater. Additionally, we also conducted a method development study for

Involvement of LSSU Undergraduate Research Students in the Research Activities: During my sabbatical, more than 100 LSSU undergraduates used the MASC Lab for a class activity (GEOL 322, NSCI 110, BIOL 223, NRES 230, MICR 315) or for undergraduate research. In the list of my disseminated works below, undergraduate coauthors are highlighted in bold. I also retain copies of all work completed in the MASC Lab displayed in the hallway outside CRW 105.

(II) Instructional Improvement Outcomes:

Based on my completion of the weeklong μXRF training course in Madison WI and our recent advances in method development, I was able to substantially improve my materials and class activities in MICR 315 for Spring 2025. New materials include image processing using custom software we developed (Nick Gordon), x-ray backscatter imaging, Laue diffraction imaging, and correlative minerology with LDIR. This gives LSSU students access to instruction in state-of-the-art imaging methodologies, some of which are only available at our facility. I also completed a user manual to assist students/new users in obtaining high quality data from our instrument.

(III) K-12 Outreach Outcomes:

As part of my sabbatical activities I coordinated with admissions and the EU-ISD to host more than 500 K-12 students and teachers at various activities (Summer 2024 & 2025). Some students participated in a tour, while other also had the opportunity for a hands on activity with the SEM (e.g. Regional Science & Engineering Fair participants). Feedback from the participants (provided through the organizers) was excellent, suggesting our outreach efforts were highly successful.

Publications:

a. Derek Wright, Benjamin J Southwell, **Emma Zabik, Shane Coykendall, Natalie Tourangeau.** Determination of Electrolytes in Sports Drinks by Microwave Plasma Atomic Emission Spectroscopy (MP-AES) December 2025, *Spectroscopy*

b. Derek Wright, Mark R. Zierden, Stephen H. Kolomyjec, Benjamin J Southwell. Applications of Micro X-Ray Fluorescence Spectroscopy in Food and Agricultural Products. January 2025, *Spectroscopy*

c. Michelle M Jarvie, Thu N. T. Nguyen, Benjamin J Southwell, Derek Wright. Integration of Whole-Genome Sequencing with ddPCR Kit for Detection of Omicron Subvariants in Wastewater in the Upper Peninsula of Michigan. October 2024. *Applied Microbiology* 4(4):1453-1463 DOI: 10.3390/applmicrobiol4040100

Conference Presentations:

d. **Shane Coykendall, Nicholas Gordon,** Stephen Kolomyjec, **Logan McQueen, Kyle Eichorn,** and Derek Wright. Application of benchtop micro x-Ray Fluorescence spectroscopy to chemical imaging of plant and animal fossils. December 2025 American Geophysical Union 2025

e. **Shane Coykendall,** Mark Zierden, **Lilyann Secord-Rider,** Benjamin Southwell, Derek Wright. Lead Bioaccumulation and Biogeochemistry at the Gaines Highway Informal Shooting Range near Kinross, Michigan. December 2025 American Geophysical Union 2025

f. **Lilyann Secord-Rider,** Mark Zierden, **Shane Coykendall,** Derek Wright. Bioaccumulation of Lead in Earthworms from Soil Contaminated by Recreational Firearm Use. December 2025 American Geophysical Union 2025

g. **Lilyann Secord-Rider, Nicholas Gordon, Shane Coykendall,** Mark Zierden, Benjamin Southwell, Derek D Wright. Evaluation of Lead and Potential Toxic Element Leaching and Subsequent Ground Water Contamination in High Permeability Soils From Recreational Firearm Usage. December 2025 American Geophysical Union 2025

h. **Nicholas Gordon, Hayley Beaudoin,** Paul R Kelso[...], Derek Wright. Laser Direct Infrared Spectroscopy Hyperspectral Imaging; Applications in Geochemical Phase Mapping and Interpretation of Multidimensional Analysis. December 2024 American Geophysical Union 2024

i. K.D.V.B. Jayawardhana, Pradeep Ranasinghe, Derek Wright. Potential new chemical and mineralogical proxies to reconstruct precipitation records using speleothems. December 2024 American Geophysical Union 2024

j. **Nicholas Gordon, Ashley Render,** Pradeep Ranasinghage[...], Derek Wright. Application of Correlative Chemical Imaging Techniques to Improve Paleoclimate Reconstruction Using Speleothems. December 2024 American Geophysical Union 2024

k. **Shane Coykendall,** Deidre Furlich, Benjamin J Southwell, Derek Wright. Assessment of PFAS sources in coastal Lake Huron waters within the US Great Lakes. December 2024 American Geophysical Union 2024

l. **Shane Coykendall,** Mark R. Zierden**, Nicholas Gordon**[...], Derek Wright. Copper Biogeochemistry and Bioaccumulation at the Historic Freda Stamp Mill near Houghton Michigan. December 2024 American Geophysical Union 2024

m. **Ashley Render, Nicholas Gordon,** Paul Kelso[...], Derek Wright. Application of Chemical Imagining Techniques to Stromatolite Fossils: Implication for Paleoenvironmental Reconstruction. December 2024 American Geophysical Union 2024

n. **Nicholas Gordon,** Ana Robbins, **Arianna DeHoyos**[...], Derek Wright. Investigation of the Spatial Variability of Heavy Metal Based Pigments in Nineteenth and Twentieth Century Books. October 2024 Upper Peninsula American Chemical Society.

o. **Shane Coykendall,** Mark R. Zierden**, Lilyann Secord-Rider**[...], Derek Wright. Bioaccumulation of Lead in plants at the Gaines Highway shooting range near Kinross, Michigan. October 2024 Upper Peninsula American Chemical Society.

p. **Nicholas Gordon,** Hari Kandel, Benjamin J Southwell, Derek Wright. Uranium Occurrence in Jacobsville Sandstone: A Reported Source Rock for Groundwater Uranium in Michigan's Upper Peninsula. June 2024 AGU WaterSciCon24.

q. **Molly Gilpatrick,** Hari Kandel, Benjamin J Southwell, Derek Wright. Studying Presence of Polycyclic Aromatic Hydrocarbons in Small Inland Lakes -Exploring Links with Motorized Boats and Human Impact. June 2024 AGU WaterSciCon24.

Boldface authors are LSSU undergraduates or recent graduates

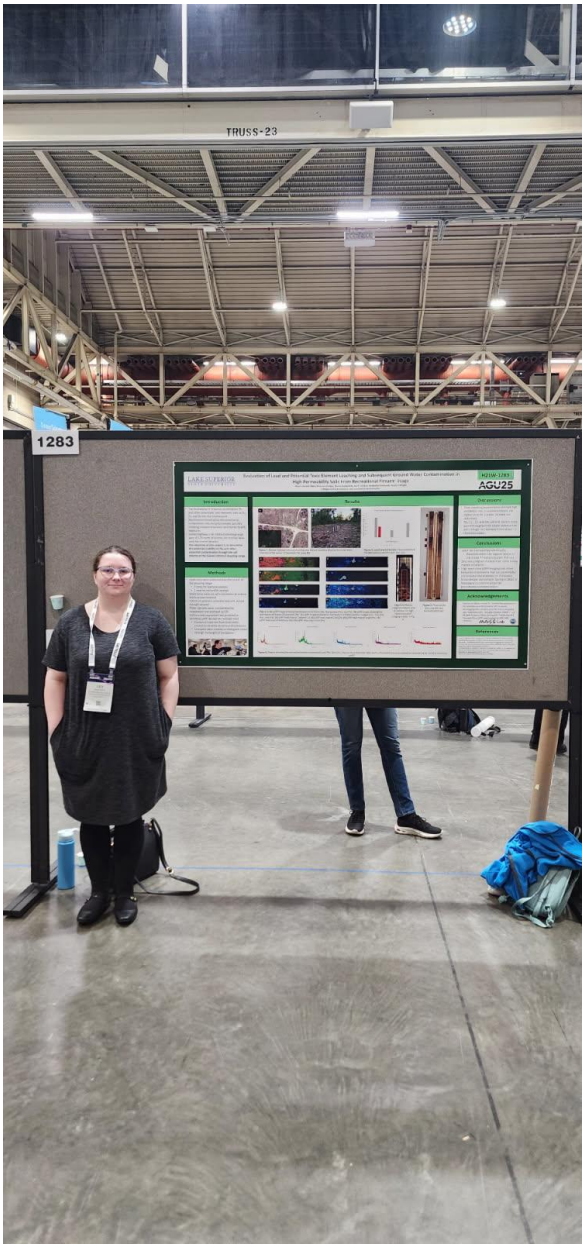

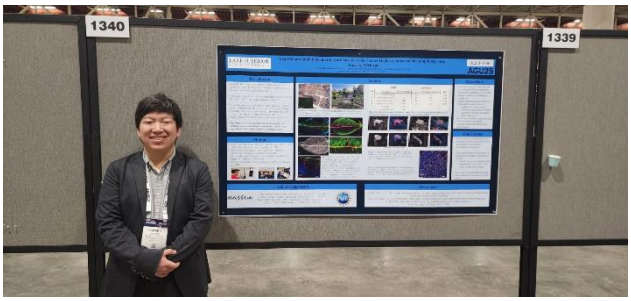

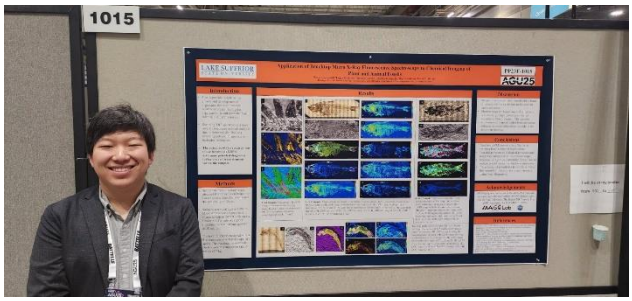

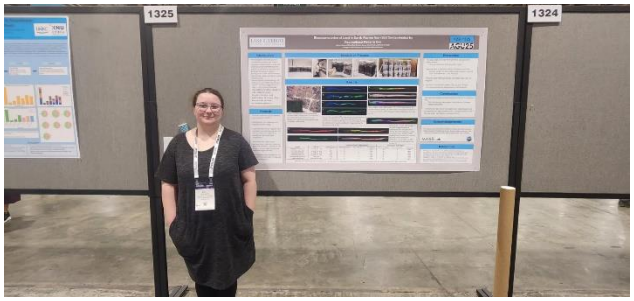

Shane Coykendall (BS Environmental Science) and Lilyann Secord-Rider (BS Biology) present their research (items d-g) at the 2025 American Geophysical Union Fall Meeting in New Orleans Louisiana.

Posters are displayed in Crawford Hall (West Basement) outside the MASC Lab (CRW 105)

Determination of Electrolytes in Sports Drinks by Microwave Plasma Atomic Emission Spectroscopy (MP-AES)

Derek D. Wright, Benjamin Southwell, Emma Zabik, Shane Coykendall, and Natalie Tourangeau.

Sports drinks, also known as electrolyte drinks, are a popular beverage choice among consumers and come in a wide variety of flavors and electrolyte compositions. They may vary substantially in their additives, which typically include sweeteners, coloring agents, flavoring agents, and additional vitamins and nutrients. The determination of electrolyte elements is important for accurate product labeling and quality control; however, conventional instrumentation, such as inductively coupled plasma optical emission spectroscopy (ICP-OES), may be costly to both acquire and operate, especially given its relatively high consumption of argon gas. Here we present a rapid and cost-effective method using microwave plasma atomic emission spectroscopy (MP-AES), which utilizes a nitrogen plasma that may be supplied with either a conventional gas source (dewar or cylinder gas) or a nitrogen generator on-site. Using a simple "dilute and shoot" method, electrolyte elements can be determined without prior sample digestion with good reproducibility and excellent limits of detection across a variety of sample matrices. Thus, MP-AES offers a simple multi-element alternative to ICP-OES for sports drink analysis without costly argon consumption.

Sports drinks are a common beverage choice, especially for those who engage in regular physical activity. While their primary purpose is to assist active people with rehydration and to replenish electrolytes lost through sweat, their use has also expanded to the general consumer beverage market. For athletes, sports drinks potentially serve a clear function. During intense or prolonged exercise, the body loses water and essential elements such as sodium, potassium, calcium, and magnesium that are crucial for maintaining muscle function and hydration. Drinking a sports beverage during or after a workout may help restore this balance, though their overall effectiveness is a matter of debate, and which formulations may be more effective is an area of active study.

Many sports drinks also contain sugar and, in some cases, caffeine, which both offer a quick energy boost. This is potentially attractive to people participating in long-distance events or high-intensity sports, where energy stores deplete quickly. By replenishing carbohydrates during the activity, athletes could potentially improve their endurance and reduce fatigue. Alternatively, many sports drink formulations contain artificial sweeteners to appeal to consumers concerned about excessive sugar consumption, leading to a wide variety of product formulations available on the consumer market. To meet product labeling requirements and provide quality control in manufacturing, there is a need for robust, low-cost methods for electrolyte element quantification that provide accurate results across a variety of product formulations.

Microwave plasma atomic emission spectrometry (MP-AES) is an emerging atomic emission technique that utilizes collisions in plasma to promote some atoms to excited electronic states from which they can emit photons as they return to lower energy states. The MP-AES instrument utilizes a microwave-induced nitrogen plasma instead of combustible gases or costly argon, allowing analysis at a fraction of the cost of traditional analytical techniques (1). During the last decade, this technique has shown promising performance as a quantitative analytical technique, with applications in fields such as geological, environmental, food, health, energy, agricultural, pharmaceuticals, and waste electrical and electronic equipment regulation (WEEE)/restriction of hazardous substances (RoHS) compliance (2-7) Thus, MP-AES offers an alternative to both atomic absorption spectroscopy (AAS) and inductively coupled plasma optical emission spectroscopy (ICP-OES) techniques

that had several advantages including improved lab safety relative to flame AAS, relatively inexpensive operating costs, multi-element capability, good speed, and good detection power; making it an efficient cost-effective analytical tool compared to previous techniques (1). The MP-AES models record emission signals sequentially. Therefore, analytical conditions can be optimized for each specific element within the same experiment, which maximizes efficiency and may minimize potential interferences (2).

The objectives of this study were to evaluate the suitability of MP-AES for the analysis of electrolyte elements in sport drinks and to develop a simple, low-cost method for routine analysis. While traditional methods often require complicated digestions before sample analysis, this study utilizes a "dilute and shoot" method for elemental analysis of Na, K, Ca, and Mg, which may be present in concentrations as high as several hundred mg/l if used in electrolyte mixtures in sports drinks.

Methods

Sample Preparation

Samples of sports drinks from five different brands in multiple varieties were obtained from a major local retailer (Walmart, Sault Sainte Marie, MI). Varieties were selected to represent different brands, sweeteners, and flavoring/coloring agents (Table I). Samples were prepared by diluting each beverage 1:500 with 2% Nitric Acid prepared from trace element certified concentrated acid (Aristar) diluted with ultrapure water. Additionally, a second sample of each beverage was prepared identically and spiked with 2mg/l of each element from a National Institute of Standards and Technology (NIST) traceable stock element standard (Inorganic Ventures).

Analysis Conditions

Samples were analyzed with an Agilent 4200 Microwave Plasma Atomic Emission Spectrometer equipped with a OneNeb Series 2 nebulizer (Agilent Technologies) and a cyclonic spray chamber, and a standard torch. The Agilent 4200 is equipped with a Czerny-Turner monochromator with 600 mm focal length and covers a spectral range of 178-780 nm. For all experiments, the nitrogen plasma was supplied from high-pressure cylinders, though dewar nitrogen or a nitrogen generator could also be utilized. Samples were introduced manually, though an autosampler can also be equipped. Additional method parameters are described in Table II.

Calibration standards were prepared in 2% nitric acid from stock element solutions covering the expected elemental range of 0.05-10 mg/l in the diluted samples. Standards were analyzed at the beginning of the analysis, with a 2 mg/l standard measured every 10 samples to monitor method performance. The built-in three-channel peristaltic pump was also utilized to introduce an internal standard solution via an online mixing tee. The solution contained rhodium (10 mg/l) to monitor for sensitivity drift and to verify the absence of matrix interferences due to variations in sample viscosity, which can negatively affect accuracy and precision. Additionally, the internal standard solution contained an excess of cesium (500 mg/l) to act as an ionization

TABLE I: Components of sports drinks utilized for method development

Sample	Brand	Sweetener	Color
1	A	Acesulfame K, sucralose	Yellow 5 & 6
2	A	High fructose corn syrup	Yellow 5 & 6
3	B	Acesulfame K, sucralose	Vegetable Juice Concentrate
4	B	Dextrose	Red 40
5	B	Sugar	Red 40
6	C	Sugar	Purple carrot juice concentrate
7	C	Natural fruit flavors	Natural colors, CI Food Orange 6 (E160e)
8	C	Natural flavor	None
9	D	Acesulfame K, sucralose	None
10	E	Sugar, Stevia	Natural vegetable juice concentrate

TABLE II: Additional Method Parameters

Rinse time: 60s	
Uptake time: 40s (fast pump enabled)	
Stabilization time: 15s	
Integration time: 3s	
Replicates:3	
Emission Lines	
Element	**Emission Line (nm)**
Na	588.995
K	766.491
Ca	393.366
Mg	280.271
Rh	343.489
Rh	437.48
Cs	455.528
Cs	672.328

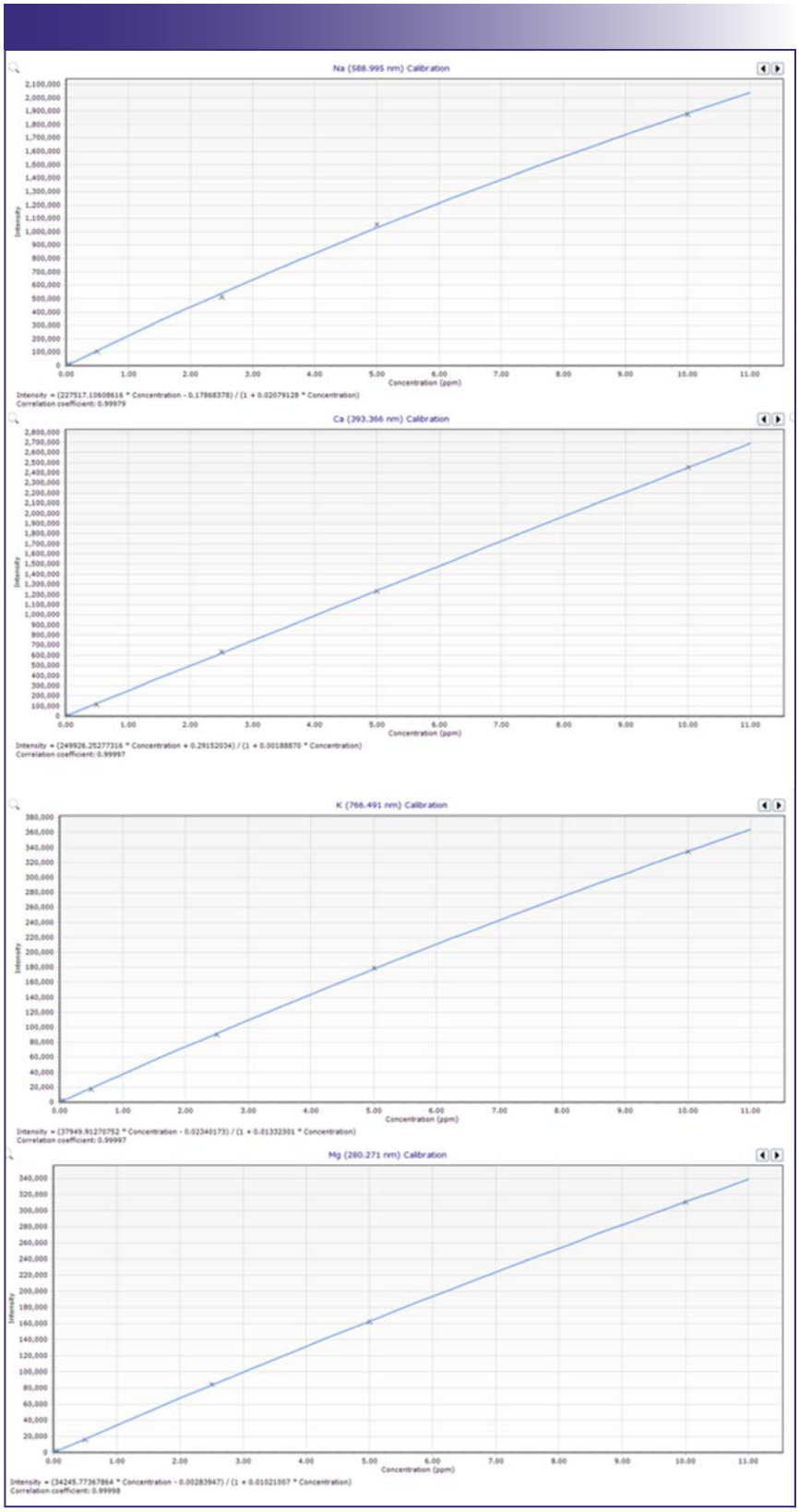

FIGURE 1: Calibration curves for sodium, potassium, calcium, and magnesium and rational curve fits using the MP Expert software (Agilent Technologies).

buffer and suppress easily ionizable element effects.

Results

Calibration Results

As instrument calibration is fundamental to producing accurate results, we carefully examined the calibration curves for each emission line during method development. The sensitivity of MP-AES is excellent for Group I (Na, K) and Group II elements (Ca, Mg), so the calibration standards were designed to bracket the samples and matrix spikes within the linear response range of the instrument. Following analysis of calibration standards, calibration curves were visually examined for linearity to determine the best calibration model. While a linear fit to the calibration curves resulted in an r^2 value of more than 0.999 for all emission lines, a slight curvilinearity could be visually detected, so the rational fit calibration model in the MP Expert software was selected for all lines, resulting in slight improvements to the r^2 values. The resulting calibration curves (Figure 1) were subsequently used for the determination of element concentrations.

Evaluation of Matrix Effects

A variety of possible matrix effects may negatively affect results by MP-AES, so several steps were taken to minimize and evaluate any possible effects on the accuracy of results. The significant sample dilution (1:500) was expected to eliminate any effects of viscosity variation on nebulizer efficiency, but to confirm this, we monitored the response of the Rh internal standard (10 mg/l) at the 343.489 and 437.480 emission lines. Across the analytical run, only minimal variation in response for both emission lines was observed, demonstrating that viscosity variations were minimal (Figure 2).

As the Agilent 4200 is an axial view design, easily ionizable element (EIE) effects are a potential concern, even with high sample dilution. The EIE effect can result when ionization in the plasma produces excess free electrons, resulting in reduced ionization of low first ionization potential elements (such as Na and K).

This subsequently results in signal enhancement for these elements, which can negatively affect accuracy.

A common strategy for reducing EIE effects is to add an excess of a low first ionization potential element, usually cesium. Excess Cs acts as an ionization buffer, ideally by providing a constant supply of excess free electrons to the plasma. In the method presented here, Cs was added at a final concentration of 500 mg/l. Variations in ionization conditions in the plasma were monitored by analysis of the Cs 455.528 and 672.328 emission lines over the course of the analytical run (Figure 3). Signal intensity for Cs lines was relatively constant (variation <10% in all samples and standards), suggesting that EIE effects were likely to be minimal.

We also evaluated each sample individually for matrix interferences by monitoring the recovery of a 2 mg/l element spike. The spike recoveries demonstrated good recovery, suggesting matrix interferences generally have minimal effect on the accuracy of the results (Table III). Sample 6 did show an unacceptably low recovery for the Ca spike. That sample contained the highest concentration of Ca (Table V), which may have impacted the spike recovery by resulting in an insufficient difference in concentration between the sample and spiked sample for accurate recovery determination.

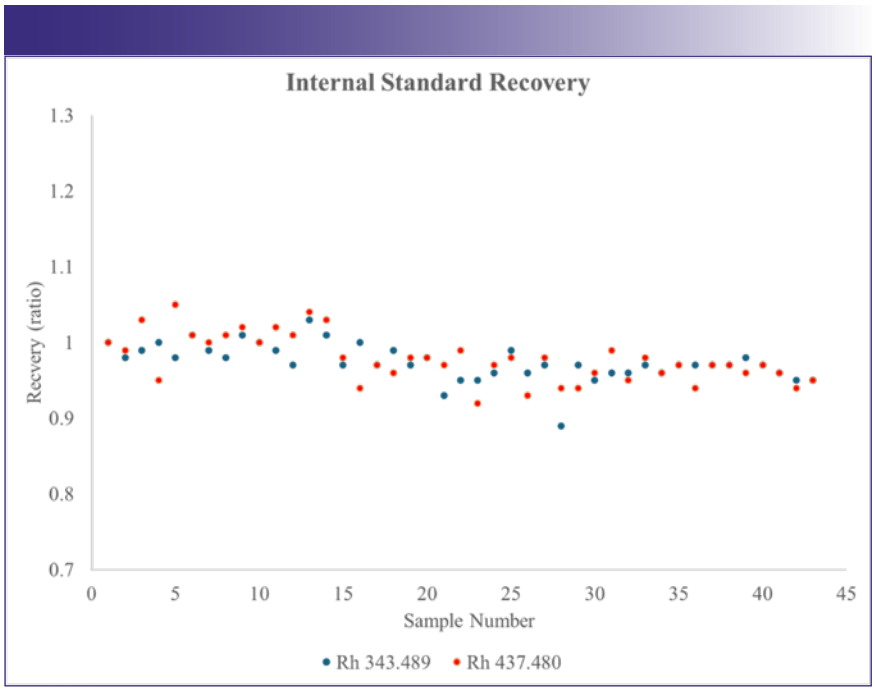

FIGURE 2: Rhodium (10 mg/L) internal standard recovery.

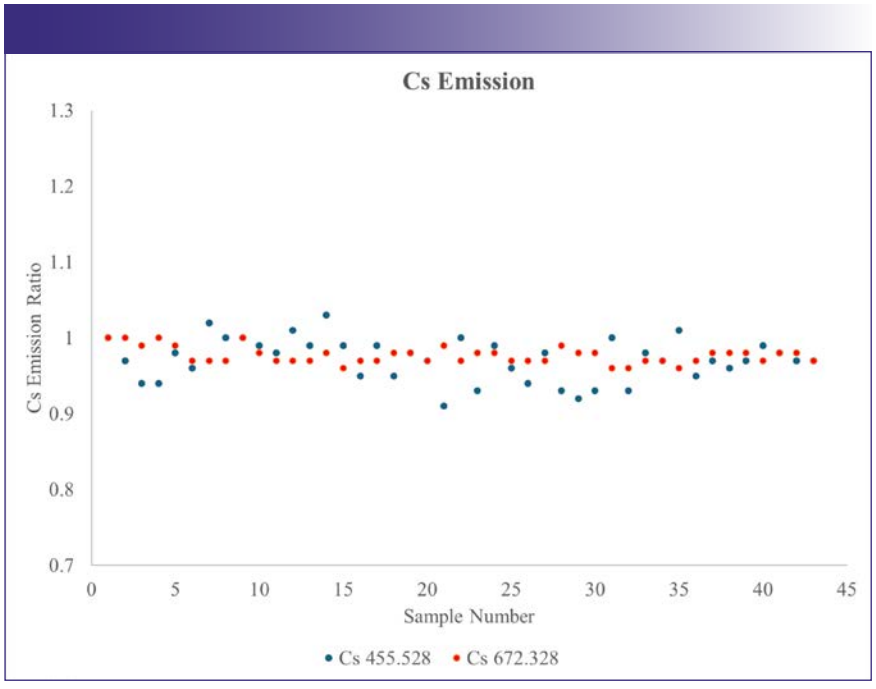

FIGURE 3: Variation in intensity of cesium emission lines over the course of sample analysis.

TABLE III: Spike recovery (%) for 2 mg/L spikes in diluted samples

		Spike Recovery (%)			
Sample	**Brand**	**Na**	**K**	**Ca**	**Mg**
1	A	92	92	92	86
2	A	97	95	93	92
3	B	101	96	95	93
4	B	94	98	102	95
5	B	96	94	103	92
6	C	106	105	63	99
7	C	98	97	98	92
8	C	98	106	103	93
9	D	94	88	103	88
10	E	93	92	99	91

TABLE IV: Method detection limits determined in diluted and undiluted samples

	Detection Limits (mg/L)	
	Diluted Sample	**Undiluted Sample**
Na	0.003	1.7
K	0.003	1.6
Ca	0.002	1
Mg	0.0009	0.43

Method Detection Limits

Method detection limits were assessed by analysis of 10 replicates of the blank solution (2% nitric acid; Table IV). Determined MDLs, even with the significant degree of dilution utilized in this method, are sufficiently low to determine electrolyte additives in sports drinks, which are often in the range of several hundred mg/l or higher.

Results from Beverage Analysis

Results of the electrolyte elements determination in the sports drinks studied here are presented in Table V. Sodium is the main electrolyte element added to most of the drink formulations studied, though significant quantities of potassium and lesser quantities of Ca and Mg are sometimes present. As sodium is the primary cation lost in sweat, it is unsurprising that most of the studied formulations utilize sodium as the primary electrolyte. The observation of alternative formulations, however (such as those with significant K), demonstrates the utility of using a multielement technique such as MP-AES, which can detect all four elements (Na, K, Ca, and Mg) when present as significant components of electrolyte mixtures.

Conclusions

MP-AES is a fast, low-cost, multielement method suitable for determining electrolyte elements in sports drinks utilizing a simple "dilute and shoot technique." Use of an internal standard and ionization buffer provides adequate control of matrix interferences in diluted samples, and the excellent sensitivity of Group I and II elements such as Na, K, Ca, and Mg allows sufficient sensitivity even with significant dilution. This makes MP-AES an attractive choice, especially for smaller labs that with lower sample throughput for which ICP-AES may prove too costly, but FAAS may be too slow (or have concerns about the safety of combustible gases).

TABLE V: Electrolyte elements in analyzed sports drinks (ND indicates the element was not detected)

		Sample Concentration (mg/L)			
Sample	**Brand**	**Na**	**K**	**Ca**	**Mg**
1	A	650	200	20	10
2	A	640	200	40	10
3	B	390	130	ND	ND
4	B	430	120	ND	ND
5	B	750	540	210	190
6	C	40	1390	890	150
7	C	30	1460	30	150
8	C	ND	1190	ND	130
9	D	30	1480	ND	270
10	E	120	1110	310	90

Acknowledgments

Funding for this work was provided by the Lake Superior State University College of Arts and Sciences.

References

(1) Hammer, M. R. A Magnetically Excited Microwave Plasma Source for Atomic Emission Spectroscopy with Performance Approaching That of the Inductively Coupled Plasma. *Spectrochim. Acta B* **2008,** *63* (4), 456–464. DOI: 10.1016/j.sab.2007.12.007

(2) Balaram, V. Microwave Plasma Atomic Emission Spectrometry (MP-AES) and its Applications – A Critical Review. *Microchem. J. 2020, 159,* 105483. DOI: 10.1016/j.microc.2020.105483.

(3) Espinosa Cruz, T. L.; Wrobel, K.; Yanez Barrientos, E.; Corrales Escobosa, A. R.; Garay-Sevilla, M. E.; Acevedo Aguilar, F. J.; Wrobel, K. Determination of Sodium, Potassium, Calcium and Magnesium in Urine, Using Microwave Plasma - Atomic Emission Spectrometry and Multi-Energy Calibration. *J. Mex. Chem. Soc.* **2024**, *68* (1), 18–28. DOI: 10.29356/jmcs.v68i1.1906

(4) Karlsson, S.; Sjöberg, V.; Ogar, A. Comparison of MP AES and ICP-MS for Analysis of Principal and Selected Trace Elements in Nitric Acid Digests of Sunflower (*Helianthus Annuus*). *Talanta* **2015**, *135*, 124–132. DOI: 10.1016/j.talanta.2014.12.015

(5) Ozbek, N.; Akman, S. Microwave Plasma Atomic Emission Spectrometric Determination of Ca, K, and Mg in Various Cheese Varieties. *Food Chem. 2016, 192*, 295–298. DOI: 10.1016/j.foodchem.2015.07.011

(6) Kerie, Y.; Hymete, A.; Ashenef, A. Analytical Method Development and Validation Based on Simple Color Reactions and Microwave Plasma–Atomic Emission Spectrometry (MP-AES) for the Detection of Adulteration in Teff Injera (Ethiopian Flatbread). *Food Anal. Methods* **2024**, *17*, 1571–1580. DOI: 10.1007/s12161-024-02684-9

(7) Vysetti, B.; Vummiti, D.; Roy, P.; Taylor, C.; Kamala, C. T.; Satyanarayanan, M. et al. Analysis of Geochemical Samples by Microwave Plasma-AES. *Atomic Spectroscopy*, **2014**, *35* (2), 65-78.

Direct correspondence regarding this article to dwright1@lssu.edu

Derek Wright is a Professor of Environmental Science and is the Facility Coordinator of the Micro Analysis and Spectroscopic Characterization at Lake Superior State University. He earned his PhD in 2008 from Rutgers University, and has expertise in both Atomic and Molecular Spectroscopy, ICP-MS, XRF, SEM-EDS, and molecular techniques.

Benjamin Southwell is an Associate Professor of Bioanalytical Chemistry and is the Facility Coordinator of the Cannabis Center of Excellence at Lake Superior State University. He earned his MA in 2013 from Central Michigan University and has expertise in in both Atomic and Molecular Spectroscopy, Mass Spectrometry, and Molecular Techniques.

Emma Zabik graduated from Lake Superior State University in May 2025 with a BS in Biology, and minors in Human Nutrition, Environmental Science, and Chemistry. Emma is currently completing requirements for the Certificate in Microscopy and Microanalysis, and plans to attend Graduate School in Fall, 2026. Her research interests are in food science and human nutrition.

Shane Coykendall is a senior at Lake Superior State University where he is pursuing a BS in Environmental Science with a Geology Minor, an Associate's Degree in Chemistry, and a Certificate in Microscopy and Microanalysis. Shane plans to attend graduate school in Fall 2026. His research Interests are in Geochemistry and environmental analysis.

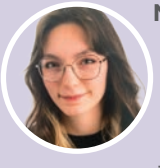

Natalie Tourangeau is a senior at Lake Superior State University where she is pursuing a BS in Chemistry with minors in Mathematics and Biochemistry. Her research interests are in microbiology and water science.

applied microbiology

MDPI

Article

Integration of Whole-Genome Sequencing with ddPCR Kit for Detection of Omicron Subvariants in Wastewater in the Upper Peninsula of Michigan

Michelle M. Jarvie *, Thu N. T. Nguyen, Benjamin Southwell and Derek Wright

School of Chemistry, Environmental, and Geosciences, Lake Superior State University, 650 W. Easterday Ave., Sault Ste. Marie, MI 49783, USA; tnguyenmosey@lssu.edu (T.N.T.N.); bsouthwell@lssu.edu (B.S.); dwright1@lssu.edu (D.W.)

* Correspondence: mjarvie1@lssu.edu

Abstract: This study explores the integration of genome sequencing and digital droplet polymerase chain reaction (ddPCR)-based methods for tracking the diversity of COVID-19 variants in wastewater. The research focuses on monitoring various Omicron subvariants during a period of significant viral evolution. Genome sequencing, particularly using Oxford Nanopore Technology (ONT), provides a detailed view of emerging variants, surpassing the limitations of PCR-based detection kits that rely on known sequences. Of the 43 samples analyzed, 39.5% showed matching results between the GT Molecular ddPCR kits and sequencing, though only 4% were exact matches. Some mismatches occurred due to newer subvariants like XBB and BQ.1, which the ddPCR kits could not detect. This emphasized the limitations of ddPCR kits, which rely on known variant sequences, while sequencing provides real-time data on emerging variants, offering a more comprehensive view of circulating strains. This study highlights the effectiveness of combining these methodologies to enhance early detection and inform public health strategies, especially in regions with limited clinical sequencing capabilities.

Keywords: COVID-19; Omicron; ddPCR; whole-genome sequencing; wastewater-based epidemiology

Citation: Jarvie, M.M.; Nguyen, T.N.T.; Southwell, B.; Wright, D. Integration of Whole-Genome Sequencing with ddPCR Kit for Detection of Omicron Subvariants in Wastewater in the Upper Peninsula of Michigan. *Appl. Microbiol.* **2024**, *4*, 1453–1463. https://doi.org/10.3390/applmicrobiol4040100

Academic Editor: Ian F. Connerton

Received: 30 August 2024
Revised: 7 October 2024
Accepted: 8 October 2024
Published: 13 October 2024

1. Introduction

The COVID-19 pandemic, caused by the SARS-CoV-2 virus, highlighted the critical need for robust epidemiological tools to monitor and mitigate the spread of infectious diseases. One of the most significant challenges in mitigating the pandemic has been the emergence and spread of viral variants, which can have altered transmissibility, virulence, and vaccine efficacy [1,2]. Genome sequencing has emerged as a pivotal technology in tracking the temporal diversity of SARS-CoV-2 variants, providing invaluable insights into the evolutionary dynamics of the virus and informing public health responses.

Genome sequencing allows for the characterization of the detailed genetic makeup of SARS-CoV-2, enabling the identification of mutations and the classification of viral lineages. This technology has been instrumental in detecting variants of concern (VOCs) and variants of interest (VOIs), such as Alpha (B.1.1.7), Delta (B.1.617.2), and Omicron (B.1.1.529), which have had significant impacts on the trajectory of the pandemic [3,4]. By analyzing the viral genome, researchers can track the emergence of these variants and their spread across different regions and time periods, providing a real-time map of viral evolution [5–7].

Wastewater-based epidemiology (WBE) has emerged as a complementary approach to clinical testing, offering a non-invasive and cost-effective means to monitor community-level infections. This method involves the collection and analysis of wastewater samples to detect the presence of SARS-CoV-2 genetic material, allowing for the early detection of outbreaks and the assessment of variant prevalence in the population [8,9]. The integration of genome sequencing with WBE has proven particularly powerful, enabling the detection

of low-frequency variants and providing a comprehensive view of viral diversity in a community [6,10–12].

Oxford Nanopore Technology (ONT) has been widely adopted for sequencing SARS-CoV-2 due to its portability, rapid turnaround time, and ability to generate long reads, which are beneficial for detecting complex variants and reconstructing viral genomes from mixed samples [9,13]. Studies employing ONT for wastewater sequencing have successfully identified and tracked the temporal diversity of SARS-CoV-2 variants, demonstrating its utility in public health surveillance and outbreak management [9,14–16].

Genome sequencing offers a more comprehensive approach to identifying COVID-19 variants compared to PCR testing, which was the pioneering tool developed to detect COVID-19 in wastewater early in the pandemic [8,17]. While PCR tests are effective in detecting the presence of the virus, they do not provide detailed information about the genetic sequence, which is crucial for identifying and tracking specific variants [18]. The PCR-based identification of COVID-19 variants is also limited to the detection of specific known mutations, whereas genome sequencing deciphers the entire genetic code of the virus, allowing researchers to detect new and emerging mutations and understand how the virus is evolving [6,16,19,20].

Few studies have compared the usefulness and accuracy of the two methods side-by-side [21], and the majority that have were using clinical nasal swabs [4,22,23], or a combination of clinical and wastewater samples [24,25]. In a review of 80 studies on COVID-19 variant determination, only 2 compared sequencing and PCR variant detection in wastewater [21,26,27]. This study aims to compare the application of genome sequencing in tracking the temporal diversity of COVID-19 variants with a commercially available quantitative polymerase chain reaction wastewater variant kit. This study occurred during a period of transition between various Omicron subvariants: BA.1, BA.2, BA.4, BA.5, XBB, and BQ.1. Additionally, the study evaluates the effectiveness of these combined methodologies in offering early warning signs for public health interventions and in understanding the geographical spread and persistence of different variants. This integrated approach is particularly relevant for informing targeted public health strategies, especially in rural areas with limited clinical sequencing capabilities. The insights gained from this study will contribute to the optimization of wastewater-based epidemiology as a valuable tool in managing current and future pandemics.

2. Materials and Methods

2.1. Study Location

Samples were gathered weekly, beginning June 2021, from 16 sites across Michigan's Eastern Upper Peninsula (EUP). The EUP includes Alger, Chippewa, Luce, Mackinac, and Schoolcraft Counties, totaling about 70,000 residents over 5566 square miles, with an average density of 11.3 people per square mile. Only 13 of the sites were included in this study: 2 did not sample during the winter due to prohibitive ice and snow cover, and 1 did not have any samples during the study period, 9 January–27 April 2023, that met the minimum criteria for genome sequencing (discussed later). Figure 1 shows the sampling site locations included in this study.

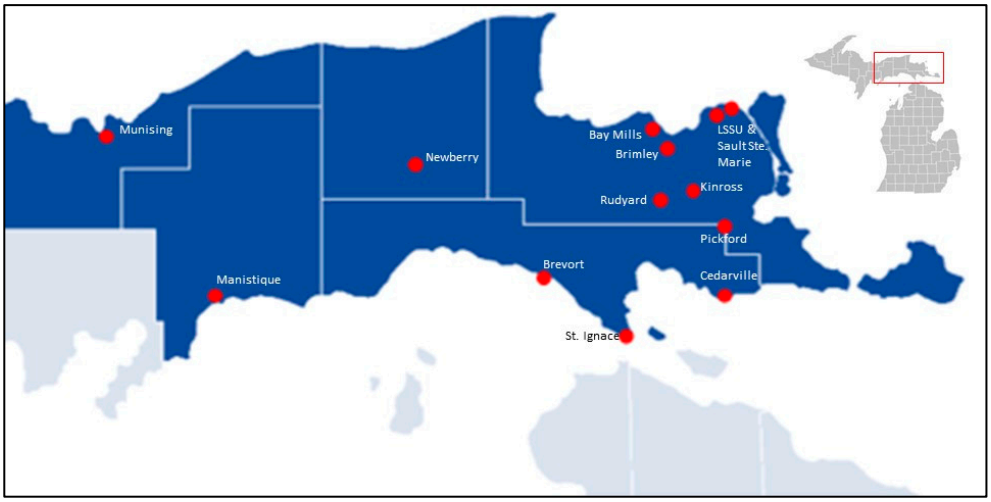

Figure 1. Sampling site locations (marked in red) in the Eastern Upper Peninsula of Michigan.

2.2. Wastewater Sampling

Wastewater grab samples (250 mL) were collected from wastewater influent streams once per week. Samples were refrigerated or kept on ice until processed (up to 48 h).

2.3. Viral Concentration

Each sample of raw sewer water (100 mL) was combined with 8% (*w*/*v*) molecular-grade polyethylene glycol (PEG) 8000 (Fisher Scientific) and 0.2 M NaCl (*w*/*v*) (Fisher Scientific) [28,29]. After mixing for two hours at 230 rpm and 4 °C, samples were centrifuged at 4200× *g* for 45 min at 4 °C [28,29]. Supernatant was removed using a sterile serological pipet, and the pellet was resuspended in 3–6 mL of residual liquid (supernatant that could not be removed without disturbing the pellet) [28,29].

2.4. RNA Extraction

Viral ribonucleic acid (RNA) was extracted from concentrated samples using the Qiagen QiAmp Viral RNA Minikit following the manufacturer's custom protocol for the QIACube Connect (Qiagen, Hilden, Germany). RNA extraction resulted in a final elution volume of 80 µL. Extracted RNA was used immediately for viral detection and quantification or stored at −80 °C for later use.

2.5. Initial Virus Detection and Quantification

Bio-Rad's One-step RT-ddPCR Advanced Kit for Probes was used with the Bio-Rad Automated Droplet Generator and the QX200 ddPCR system to quantify N1, N2, and Phi6 RNA (Bio-Rad, Hercules, CA, USA). Each reaction contained a final concentration of 1× Supermix (Bio-Rad, USA), 20 U/µL reverse transcriptase (RT) (Bio-Rad, USA), 15 nM DTT (Bio-Rad, Hercules, CA), 900 nmol of each primer (BioSearch Tech, Novato, CA), 250 nmol of each probe (BioSearch Tech, Novato, CA, USA), 1 µL of nuclease-free water, and 5.5 µL of template RNA. See the Supplementary Information for primer/probe sequences. The final reaction volume was 22 µL. Quality control samples on each plate included a non-template control, extraction control (elution buffer spiked with Phi6), and processing blank (water spiked with Phi6). Samples, controls, and blanks were analyzed in triplicate.

Droplets were generated in the Bio-Rad Automated Droplet Generator (ADG) by combining 20 µL of reaction volume with 70 µL of droplet generator oil (Bio-Rad, USA), resulting in a reaction mixture–oil emulsion of 40 µL containing up to 20,000 droplets. The droplets were transferred, via the ADG, to a 96-well PCR plate that was then heat-sealed with foil and put in a Bio-Rad C1000 deep-well thermal cycler for PCR amplification under the following conditions: 25 °C for 3 min, 50 °C for 60 min, 95 °C for 10 min, 40 cycles of 95 °C for 30 s and 55 °C for 1 min, 98 °C for 10 min, and hold at 4 °C.

After thermal cycling, the plate was transferred to the Bio-Rad QX200 Droplet Reader for concentration determination via the spectrophotometric detection of fluorescent probe signal in gene-target positive droplets. Amplitude thresholding was performed manually for each analysis using the QuantaSoft (BioRad, Hercules, CA) software (version 1.7). Lower limit of detection (see Supplementary Information), N1, N2, and Phi6 gene copies for each sample were then determined using the QuantaSoft output.

2.6. Variant Determination Using ddPCR

Samples that were N1- or N2-positive in the initial detection were then tested for variant detection using the BA.1 (A67V; del69-70 mutations) and BA.2 (R408S mutation) discrimination assay kit (GT Molecular). Each reaction contained 5.5 µL Supermix (Bio-Rad, USA), 2.2 µL reverse transcriptase (RT) (Bio-Rad, USA), 1.1 µL DTT (Bio-Rad, USA), 1 µL GT primer-probe solution (GT Molecular), 6.7 µL of nuclease-free water, and 5.5 µL of template RNA for a total reaction volume of 22 µL. Droplet generation was performed in the same manner as previously described. Thermal cycling conditions were as follows: 50 °C for 60 min, 95 °C for 10 min, 45 cycles of 94 °C for 30 s and 60 °C for 1 min, 98 °C for 10 min, and hold at 4 °C for 30 min. Concentration and target gene copies were determined in the same manner as described above for N1/N2 determination.

2.7. Variant Determination Using Genome Sequencing

Previously extracted RNA was used for genome sequencing. Sequencing was performed, retrospectively, several months after ddPCR variant detection. Only samples with an N1 and N2 combined concentration of ≥9000 gene copies (GC) per 100 mL were sequenced [30]. Forty-three samples during the study period (9 January–27 April 2023) met these criteria for sequencing.

Reverse transcription was performed using the Midnight RT PCR Expansion kit (EXP-MRT001, Oxford Nanopore Technologies, Oxford, UK). An input volume of 8 µL of sample RNA was mixed with 2 µL LunaScript RT Supermix and then thermal cycled in the following conditions: 25 °C for 2 min, 55 °C for 10 min, 95 °C for 1 min, and hold at 4 °C. Midnight primer pools A and B were then mixed according to the manufacturer protocol and aliquoted 10 µL each into a clean 96-well plate. To each primer pool, 2.5 µL of RT reaction was added. Thermal cycling was performed under the following conditions: 98 °C for 30 s, 35 cycles of 98 °C for 30 s, 61 °C for 2 min, 65 °C for 3 min, and hold at 4 °C.

The addition of barcodes was performed according to the manufacturer's protocol using the Rapid Barcoding kit (SQK-RBK110.96, Oxford Nanopore Technologies). For each sample, 2.5 µL from primer pools A and B was combined with 2.5 µL or nuclease-free water in a clean 96-well plate. Then, 2.5 µL of Rapid Barcode was added to the corresponding sample wells. The barcoded plate was incubated at 39 °C for 2 min and then 88 °C for 2 min. Barcoded samples were then pooled in a clean Eppendorf DNA LoBind tube. Half of the pooled sample was used and half was stored at 4 °C in a case needed for reloading during the sequencing run. To the pooled, barcoded sample, an equal volume of AMPure XP Beads were added and then mixed on a rotator mixer at room temperature for five minutes. After mixing, the tube was put on a magnet and the beads were washed twice with 1 mL of 80% ethanol. Residual ethanol was discarded, and the pellet was resuspended with 15 µL of elution buffer and incubated at room temperature for 10 min. Up to 800 ng of DNA library was transferred to a clean tube and combined with 1 µL of Rapid Adaptor F.

The prepared DNA library was combined with 37.5 µL Sequencing Buffer and 25.5 µL Loading Beads and loaded into a MinION R9.4.1 flow cell which was placed onto a MinION Mk1C sequencer (Oxford Nanopore Technologies) for 24–72 h using the MinKNOW software (version 23.04.5) (min accepted quality score 8, minimum 200 bp read length). Data were analyzed using EPI2ME's (Oxford Nanopore Technologies) FastqQC + ARTIC + NextClade workflow with the ARTIC nCoV-2019 protocol.

3. Results and Discussion

During the study period, N1 + N2 gene copies fluctuated between 1163 and 2.8 million, with a mean of 32,127 and a median of 3607. Of the 210 samples tested from the 13 included sites, 43 met the minimum criteria of 9000 N1 + N2 combined gene copies. Figure 2 shows the normalized N1 + N2 gene copies by site over the study period.

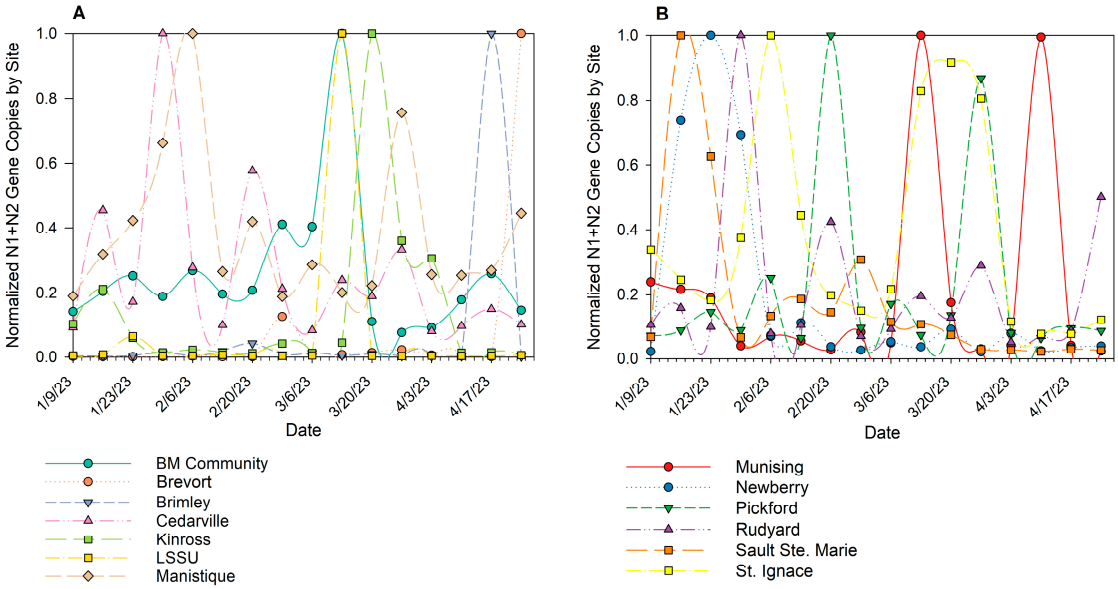

Figure 2. Normalized N1 + N2 gene copies per 100 mL by site during the study period week of 9 January 2023 through the week of 24 April 2023. Sites were separated (**A**,**B**), alphabetically, to improve data visualization.

All of the samples sequenced contained genetic markers from the Omicron family of subvariants. Of the 43 samples compared, 39.5% of the samples had matching results between the GT Molecular ddPCR kits and ONT sequencing. Of these, 4% were an exact match, and 33.5% were an "assumed" match, meaning that if the GT kit gave positive results for both BA.1 and BA.2, it was possible that BA.4 or BA.5 were present based on shared mutations among the four subvariants [31,32]. Seven percent of the samples did not register a positive result in the GT Molecular kit (<LOD) but were assigned a clade (a group of similar viruses based on genetics) using sequencing. Two of those seven were identified as BA.2 and one as recombinant. The remaining 53.5% of the samples were not matched with the two methods utilized. The majority of non-matches were assigned as "recombinant" using sequencing (35%). Others were BA.3, XBB, and BQ.1, for which there existed no markers in the GT Molecular kit being used (see Table 1).

The period of January through April 2023 saw several Omicron subvariants circulating in the Midwest region of the United States, including BA.2, BA.4, BA.5, XBB, and BQ.1, with the dominant subvariant being XBB [33]. Although BA.4/5 variant ddPCR kits were available at the time of initial analysis, BA.1/2 kits were still being used while transitioning to genome sequencing. Furthermore, the frequency of BA.2, BA.2.12.1, BA.4, and BA.5, all BA.2 relatives, fluctuated during this transition period, making the BA.2 kits still relevant [32]. The paired sequencing and ddPCR data illustrate the temporal limitations of using ddPCR variant kits alone to determine current circulating COVID-19 variants. While BA.2 was a common subvariant in circulation in the study region during the study period, early instances of XBB (1/18/23) and BQ.1 (1/30/23) in the region were missed during initial ddPCR analysis (see Table 2). These results reflect that even though BA.4/BA.5 ddPCR kits were available, the incidence of newer Omicron subvariants like XBB and BQ.1 would still have been missed because the ddPCR kits were not capable of detecting those

variants at that time. Figure 3 shows the temporal occurrence of subvariants determined by ddPCR and ONT methods.

Table 1. Comparison of subvariants identified using Oxford Nanopore Technologies sequencing and GT Molecular ddPCR BA.1/BA.2 discrimination kit over the study period 9 January–27 April 2023. The number of sequencing instances was dependent upon meeting the 9000 N1 + N2 gene copies per 100 mL minimum.

DATE	SITE	ONT	ddPCR KIT
3/14/2023	Bay Mills Community	BA.5	BA.1 and BA.2 (4/5)
3/1/2023	Brevort	BA.3	BA.2
3/8/2023	Brevort	BA.2	BA.2
3/15/2023	Brevort	BA.5	BA.1 and BA.2 (4/5)
3/22/2023	Brevort	BA.5	BA.1 and BA.2 (4/5)
3/29/2023	Brevort	BA.2	BA.1 and BA.2 (4/5)
4/5/2023	Brevort	BA.5	BA.1 and BA.2 (4/5)
4/26/2023	Brevort	XBB	BA.2
1/31/2023	Brimley	Recombinant	BA.2
3/7/2023	Brimley	Recombinant	BA.2
4/18/2023	Brimley	XBB	BA.2
2/2/2023	Cedarville	BQ.1	BA.1 and BA.2 (4/5)
2/23/2023	Cedarville	BA.2.10	BA.2
1/10/2023	Kinross	BA.5	BA.1 and BA.2 (4/5)
2/28/2023	Kinross	Recombinant	BA.1 and BA.2 (4/5)
3/14/2023	Kinross	Recombinant	BA.2
3/21/2023	Kinross	BA.2.10	BA.2
3/28/2023	Kinross	BA.2.10	BA.2
4/4/2023	Kinross	BA.2	BA.2
3/15/2023	LSSU	BA.2.10	BA.2
1/30/2023	Manistique	BQ.1	BA.1 and BA.2 (4/5)
3/20/2023	Manistique	BA.2	<LOD
1/23/2023	Munising	Recombinant	BA.2
3/13/2023	Munising	BA.2	BA.2
3/20/2023	Munising	Recombinant	BA.1 and BA.2 (4/5)
4/10/2023	Munising	XBB	BA.2
1/31/2023	Newberry	BA.5	BA.1 and BA.2 (4/5)
2/14/2023	Newberry	Recombinant	<LOD
4/4/2023	Newberry	Recombinant	<LOD
2/22/2023	Pickford	BA.2	BA.2
3/29/2023	Pickford	BA.5	BA.1 and BA.2 (4/5)
2/2/2023	Rudyard	BQ.1	BA.1 and BA.2 (4/5)
2/23/2023	Rudyard	Recombinant	BA.2
3/30/2023	Rudyard	Recombinant	BA.2
4/27/2023	Rudyard	XBB	BA.2
1/18/2023	Sault Ste. Marie	XBB	BA.2
1/24/2023	Sault Ste. Marie	Recombinant	BA.1 and BA.2 (4/5)
2/14/2023	Sault Ste. Marie	Recombinant	BA.2
2/28/2023	Sault Ste. Marie	Recombinant	BA.2
2/8/2023	St. Ignace	XBB	BA.2
3/15/2023	St. Ignace	BA.2	BA.2
3/22/2023	St. Ignace	Recombinant	BA.1 and BA.2 (4/5)
3/29/2023	St. Ignace	BA.2.10	BA.2

Table 2. Percent of samples (n = 43) identified as each subvariant using ONT sequencing and GT Molecular ddPCR kit.

SUBVARIANT	ONT	ddPCR KIT
BA.2	28%	58%
BA.3	2%	0%
BA.4 or BA.5	14%	25%
XBB	14%	0%
BQ.1	7%	0%
Recombinant	35%	0%
<LOD	N/A	7%

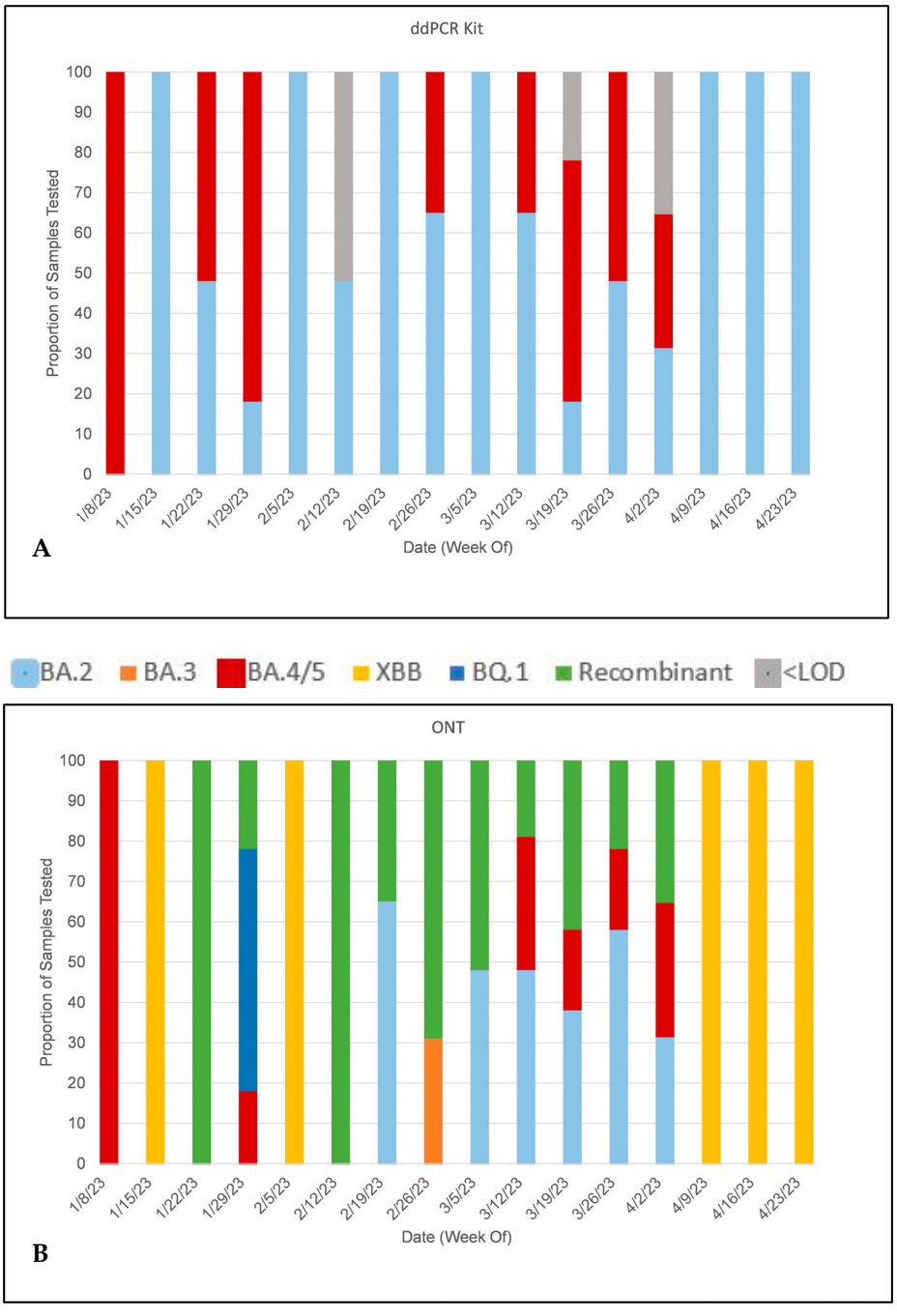

Figure 3. Comparison of temporal subvariant occurrence between ddPCR (**A**) and ONT (**B**) methods for study period 9 January 2023 through 27 April 2023.

Although more sensitive to detecting key spike protein mutations [16], ddPCR kits for detecting COVID-19 variants have a significant limitation: they rely on the specific genetic sequences of known variants. Consequently, these kits require that a variant is already in circulation before materials can be created to detect it. This limitation means that ddPCR kits might not be effective in identifying new variants immediately as they emerge, potentially delaying the detection and tracking of these new strains [34,35]. Furthermore, recent variants of concern contain more than 30 mutations in the spike protein, complicating the detection of these variants and enhancing their ability to evade detection by standard testing methods like ddPCR [36]. In contrast, genome sequencing incorporates data from global sequencing efforts, often within days of new sequences being submitted [37]. This allows for real-time tracking and analysis of SARS-CoV-2 variants, providing insights into the virus's spread and evolution without the delay for the development of new detection materials [6,16].

Another advantage of sequencing wastewater samples is that it can provide data at a population scale in places where sequencing clinical samples is limited by resources [12,38], especially when overall clinical testing has declined significantly [39,40]. During the study period, the Michigan department of Health and Human Services reports that only two clinical samples from the entire region were sequenced (S.S., personal communication, 6/18/2024). Given that there were at least five different subvariants circulating at the time, each with potentially differing transmission and virulence characteristics, sequencing only two samples would provide little information about the distribution pattern and evolution of the virus across an expansive geographic region like the Eastern Upper Peninsula of Michigan.

4. Conclusions

In summary, using PCR for the initial detection and quantification of COVID-19 virus particles in wastewater remains one of the most effective, time-efficient, and cost-efficient methods for monitoring the virus within a population [41,42]. While PCR-based variant detection kits are highly sensitive to spike protein mutations [16], they depend on known genetic sequences, resulting in delays in identifying emerging variants [34,35]. In contrast, genome sequencing technologies like ONT offer early insights into new and emerging variants spreading within communities, surpassing the capabilities of variant-specific PCR tests [16]. This study underscores the value of ONT sequencing of wastewater in providing real-time information about dominant circulating variants, equipping health officials with critical data for making targeted and effective public health decisions. Real-time data are particularly crucial in regions like the Upper Peninsula of Michigan, where limited clinical samples are sequenced. Both methods provide data about circulating variants, but ONT provides a more complete picture in rapidly evolving COVID-19 scenarios by detecting individual mutations, which allows for the identification of any current variant as well as emerging or yet-unknown variants or subvariants. This is especially helpful during transitions between highly related subvariants like the BA.2/BA.4/BA.5 family.

Supplementary Materials: The following supporting information can be downloaded at https://www.mdpi.com/article/10.3390/applmicrobiol4040100/s1: Primer and Probes Sequences for ddPCR Detection, and ddPCR Limit of Detection Calculation.

Author Contributions: Conceptualization, M.M.J., T.N.T.N., B.S. and D.W.; formal analysis, M.M.J.; writing—original draft preparation, M.M.J.; writing—review and editing, M.M.J., T.N.T.N., B.S. and D.W.; project administration, T.N.T.N., B.S. and D.W. All authors have read and agreed to the published version of the manuscript.

Funding: Funding was provided by the Michigan Department of Health and Human Services via the Epidemiology and Laboratory Capacity: Enhancing Detection Expansion through Coronavirus Response and Relief Supplemental Appropriations Act of 2021 (P.L. 116-260).

Data Availability Statement: Data available upon request from corresponding author.

Conflicts of Interest: The authors declare no conflicts of interest. The funders had no role in the design of the study; in the collection, analyses, or interpretation of the data; in the writing of the manuscript; or in the decision to publish the results.

References

1. Kaku, Y.; Okumura, K.; Padilla-Blanco, M.; Kosugi, Y.; Uriu, K.; Hinay, A.A.; Chen, L.; Plianchaisuk, A.; Kobiyama, K.; Ishii, K.J.; et al. Virological characteristics of the SARS-CoV-2 JN.1 variant. *Lancet Infect. Dis.* **2024**, *24*, e82. [CrossRef] [PubMed]
2. Kunal, S.; Ish, P.; Aditi; Gupta, K. Emergence of COVID-19 variants its global impact. In *Frontiers of COVID-19: Scientific and Clinical Aspects of the Novel Coronavirus 2019*; Adibi, S., Griffin, P., Sanicas, M., Rashidi, M., Lanfranchi, F., Eds.; Springer International Publishing: Berlin/Heidelberg, Germany, 2022; pp. 183–201. [CrossRef]
3. Viana, R.; Moyo, S.; Amoako, D.G.; Tegally, H.; Scheepers, C.; Althaus, C.L.; Anyaneji, U.J.; Bester, P.A.; Boni, M.F.; Chand, M.; et al. Rapid epidemic expansion of the SARS-CoV-2 Omicron variant in southern Africa. *Nature* **2022**, *603*, 679–686. [CrossRef] [PubMed]
4. Wang, R.; Chen, J.; Gao, K.; Hozumi, Y.; Yin, C.; Wei, G.-W. Analysis of SARS-CoV-2 mutations in the United States suggests presence of four substrains and novel variants. *Commun. Biol.* **2021**, *4*, 228. [CrossRef]
5. Davis, C.; Logan, N.; Tyson, G.; Orton, R.; Harvey, W.T.; Perkins, J.S.; Mollett, G.; Blacow, R.M.; Peacock, T.P.; Barclay, W.S.; et al. Reduced neutralisation of the Delta (B.1.617.2) SARS-CoV-2 variant of concern following vaccination. *PLoS Pathog.* **2021**, *17*, e1010022. [CrossRef] [PubMed]
6. Pilapil, J.D.; Notarte, K.I.; Yeung, K.L. The dominance of co-circulating SARS-CoV-2 variants in wastewater. *Int. J. Hydrogen Environ. Health* **2023**, *253*, 114224. [CrossRef]
7. Rothman, J.A.; Saghir, A.; Zimmer-Faust, A.G.; Langlois, K.; Raygoza, K.; Steele, J.A.; Griffith, J.F.; Whiteson, K.L. Longitudinal sequencing and variant detection of SARS-CoV-2 across southern California wastewater. *Appl. Microbiol.* **2024**, *4*, 635–649. [CrossRef]
8. Ahmed, W.; Bivins, A.; Simpson, S.L.; Bertsch, P.M.; Ehret, J.; Hosegood, I.; Metcalfe, S.S.; Smith, W.J.M.; Thomas, K.V.; Tynan, J.; et al. Wastewater surveillance demonstrates high predictive value for COVID-19 infection on board repatriation flights to Australia. *Environ. Int.* **2022**, *158*, 106938. [CrossRef]
9. Barbé, L.; Schaeffer, J.; Besnard, A.; Jousse, S.; Wurtzer, S.; Moulin, L.; Le Guyader, F.S.; Desdouits, M.; Bailly, J.-L.; Gantzer, C.; et al. SARS-CoV-2 whole-genome sequencing using Oxford Nanopore Technology for variant monitoring in wastewaters. *Front. Microbiol.* **2022**, *13*, 889811. [CrossRef]
10. Bar-Or, I.; Weil, M.; Indenbaum, V.; Bucris, E.; Bar-Ilan, D.; Elul, M.; Levi, N.; Aguvaev, I.; Cohen, Z.; Shirazi, R.; et al. Detection of SARS-CoV-2 variants by genomic analysis of wastewater samples in Israel. *Sci. Total Environ.* **2021**, *789*, 148002. [CrossRef]
11. Cancela, F.; Ramos, N.; Smyth, D.S.; Etchebehere, C.; Berois, M.; Rodríguez, J.; Rufo, C.; Alemán, A.; Borzacconi, L.; López, J.; et al. Wastewater surveillance of SARS-CoV-2 genomic populations on a country-wide scale through targeted sequencing. *PLoS ONE* **2023**, *18*, e0284483. [CrossRef]
12. Crits-Christoph, A.; Kantor, R.S.; Olm, M.R.; Whitney, O.N.; Al-Shayeb, B.; Lou, Y.C.; Flamholz, A.; Kennedy, L.C.; Greenwald, H.; Hinkle, A.; et al. Genome sequencing of sewage detects regionally prevalent SARS-CoV-2 variants. *mBio* **2021**, *12*, e02703-20. [CrossRef] [PubMed]
13. Tyson, J.R.; James, P.; Stoddart, D.; Sparks, N.; Wickenhagen, A.; Hall, G.; Choi, J.H.; Lapointe, H.; Kamelian, K.; Smith, A.D.; et al. Improvements to the ARTIC multiplex PCR method for SARS-CoV-2 genome sequencing using nanopore. *bioRxiv* **2020**. [CrossRef]
14. Izquierdo-Lara, R.; Elsinga, G.; Heijnen, L.; Munnink, B.B.O.; Schapendonk, C.M.E.; Nieuwenhuijse, D.; Kon, M.; Lu, L.; Aarestrup, F.M.; Lycett, S.; et al. Monitoring SARS-CoV-2 Circulation and diversity through community wastewater sequencing, the Netherlands and Belgium. *Emerg. Infect. Dis.* **2021**, *27*, 1405–1415. [CrossRef]
15. Nemudryi, A.; Nemudraia, A.; Wiegand, T.; Surya, K.; Buyukyoruk, M.; Cicha, C.; Vanderwood, K.K.; Wilkinson, R.; Wiedenheft, B. Temporal detection and phylogenetic assessment of SARS-CoV-2 in municipal wastewater. *Cell Rep. Med.* **2020**, *1*, 100098. [CrossRef] [PubMed]
16. Vigil, K.; D'Souza, N.; Bazner, J.; Cedraz, F.M.-A.; Fisch, S.; Rose, J.B.; Aw, T.G. Long-term monitoring of SARS-CoV-2 variants in wastewater using a coordinated workflow of droplet digital PCR and nanopore sequencing. *Water Res.* **2024**, *254*, 121338. [CrossRef]
17. Medema, G.; Heijnen, L.; Elsinga, G.; Italiaander, R.; Brouwer, A. Presence of SARS-Coronavirus-2 RNA in sewage and correlation with reported COVID-19 prevalence in the early stage of the epidemic in the Netherlands. *Environ. Sci. Technol. Lett.* **2020**, *7*, 511–516. [CrossRef]
18. World Health Organization. Methods-for-the-detection-char-SARS-CoV-2-variants_2nd update_final.pdf (pp. 1–14) [Technical Report]. 2022. Available online: https://www.ecdc.europa.eu/sites/default/files/documents/Methods-for-the-detection-char-SARS-CoV-2-variants_2nd%20update_final.pdf (accessed on 23 July 2024).

19. Child, H.T.; Airey, G.; Maloney, D.M.; Parker, A.; Wild, J.; McGinley, S.; Evens, N.; Porter, J.; Templeton, K.; Paterson, S.; et al. Comparison of metagenomic and targeted methods for sequencing human pathogenic viruses from wastewater. *mBio* **2023**, *14*, e01468-23. [CrossRef]
20. Joshi, M.; Kumar, M.; Srivastava, V.; Kumar, D.; Rathore, D.S.; Pandit, R.; Graham, D.W.; Joshi, C.G. Genetic sequencing detected the SARS-CoV-2 delta variant in wastewater a month prior to the first COVID-19 case in Ahmedabad (India). *Environ. Pollut.* **2022**, *310*, 119757. [CrossRef]
21. Tiwari, A.; Adhikari, S.; Zhang, S.; Solomon, T.B.; Lipponen, A.; Islam, M.A.; Thakali, O.; Sangkham, S.; Shaheen, M.N.F.; Jiang, G.; et al. Tracing COVID-19 trails in wastewater: A systematic review of SARS-CoV-2 surveillance with viral variants. *Water* **2023**, *15*, 1018. [CrossRef]
22. Lind, A.; Barlinn, R.; Landaas, E.T.; Andresen, L.L.; Jakobsen, K.; Fladeby, C.; Nilsen, M.; Bjørnstad, P.M.; Sundaram, A.Y.M.; Ribarska, T.; et al. Rapid SARS-CoV-2 variant monitoring using PCR confirmed by whole genome sequencing in a high-volume diagnostic laboratory. *J. Clin. Virol.* **2021**, *141*, 104906. [CrossRef]
23. Umunnakwe, C.; Makatini, Z.; Maphanga, M.; Mdunyelwa, A.; Mlambo, K.M.; Manyaka, P.; Nijhuis, M.; Wensing, A.; Tempelman, H. Evaluation of a commercial SARS-CoV-2 multiplex PCR genotyping assay for variant identification in resource-scarce settings. *PLoS ONE* **2022**, *17*, e0269071. [CrossRef]
24. D'Agostino, Y.; Rocco, T.; Ferravante, C.; Porta, A.; Tosco, A.; Cappa, V.M.; Lamberti, J.; Alexandrova, E.; Memoli, D.; Terenzi, I.; et al. Rapid and sensitive detection of SARS-CoV-2 variants in nasopharyngeal swabs and wastewaters. *Diagn. Microbiol. Infect. Dis.* **2022**, *102*, 115632. [CrossRef] [PubMed]
25. Tangwangvivat, R.; Wacharapluesadee, S.; Pinyopornpanish, P.; Petcharat, S.; Hearn, S.M.; Thippamom, N.; Phiancharoen, C.; Hirunpatrawong, P.; Duangkaewkart, P.; Supataragul, A.; et al. SARS-CoV-2 variants detection strategies in wastewater samples collected in the Bangkok metropolitan region. *Viruses* **2023**, *15*, 876. [CrossRef] [PubMed]
26. Oh, C.; Sashittal, P.; Zhou, A.; Wang, L.; El-Kebir, M.; Nguyen, T.H. Design of SARS-CoV-2 variant-specific PCR assays considering regional and temporal characteristics. *Appl. Environ. Microbiol.* **2022**, *88*, e02289-21. [CrossRef] [PubMed]
27. Rasmussen, L.D.; Richter, S.R.; Midgley, S.E.; Franck, K.T. Detecting SARS-CoV-2 Omicron, B.1.1.529 Variant in Wastewater Samples by Using Nanopore Sequencing. Available online: https://stacks.cdc.gov/view/cdc/118192 (accessed on 31 July 2024).
28. Borchardt, M.A.; Boehm, A.B.; Salit, M.; Spencer, S.K.; Wigginton, K.R.; Noble, R.T. The Environmental Microbiology Minimum Information (EMMI) Guidelines: qPCR and dPCR Quality and Reporting for Environmental Microbiology. *Environ. Sci. Technol.* **2021**, *55*, 10210–10223. [CrossRef]
29. Flood, M.; D'Souza, N.; Ives, R.; Aw, T.G.; Roase, J. Standard Operating Procedure for Sampling, Concentration and Detection of SARS-CoV-2 in Sewage. Available online: https://www.google.com/url?sa=t&source=web&rct=j&opi=89978449&url=https://s3.amazonaws.com/pf-upload-01/u-4256/0/2021-06-22/ux22lt2/SOP_SARS-CoV2%2520in%2520sewage%2520Rose%2520Lab_MSU_v2021draft_06.18.21.pdf&ved=2ahUKEwj__ODNmYqJAxUCgVYBHSdRMOk4ChAWegQIKRAB&usg=AOvVaw1Bx8U-J9bTDy5SGPJcfsh_ (accessed on 23 July 2024).
30. Gregory, D.A.; Wieberg, C.G.; Wenzel, J.; Lin, C.-H.; Johnson, M.C. Monitoring SARS-cov-2 populations in wastewater by amplicon sequencing and using the novel program SAM Refiner. *Viruses* **2021**, *13*, 1647. [CrossRef]
31. Focosi, D.; Quiroga, R.; McConnell, S.; Johnson, M.C.; Casadevall, A. Convergent evolution in SARS-cov-2 spike creates a variant soup from which new COVID-19 waves emerge. *Int. J. Mol. Sci.* **2023**, *24*, 2264. [CrossRef]
32. Pastorio, C.; Noettger, S.; Nchioua, R.; Zech, F.; Sparrer, K.M.J.; Kirchhoff, F. Impact of mutations defining SARS-CoV-2 Omicron subvariants BA.2.12.1 and BA.4/5 on Spike function and neutralization. *iScience* **2023**, *26*, 108299. [CrossRef]
33. Biobot Analytics. COVID-19, Influenza, and RSV Wastewater Monitoring in the U.S. Available online: https://biobot.io/data/ (accessed on 1 May 2023).
34. Gupta, S.; Kumar, A.; Gupta, N.; Bharti, D.R.; Aggarwal, N.; Ravi, V. A two-step process for in silico screening to assess the performance of qRTPCR kits against variant strains of SARS-CoV-2. *BMC Genom.* **2022**, *23*, 755. [CrossRef]
35. Sharma, S.; Shrivastava, S.; Kausley, S.B.; Rai, B.; Pandit, A.B. Coronavirus: A comparative analysis of detection technologies in the wake of emerging variants. *Infection* **2023**, *51*, 1–19. [CrossRef]
36. Dip, S.D.; Sarkar, S.L.; Setu, M.A.A.; Das, P.K.; Pramanik, M.H.A.; Alam, A.S.M.R.U.; Al-Emran, H.M.; Hossain, M.A.; Jahid, I.K. Evaluation of RT-PCR assays for detection of SARS-CoV-2 variants of concern. *Sci. Rep.* **2023**, *13*, 2342. [CrossRef] [PubMed]
37. Nextstrain. Nextstrain Annual Update March 2024. 2024. Available online: https://nextstrain.org/blog/2024-03-27-annual-update-march-2024 (accessed on 23 July 2024).
38. Fontenele, R.S.; Kraberger, S.; Hadfield, J.; Driver, E.M.; Bowes, D.; Holland, L.A.; Faleye, T.O.C.; Adhikari, S.; Kumar, R.; Inchausti, R.; et al. High-throughput sequencing of SARS-CoV-2 in wastewater provides insights into circulating variants. *Water Res.* **2021**, *205*, 117710. [CrossRef] [PubMed]
39. Rader, B.; Gertz, A.; Iuliano, A. Use of at-home Covid-19 tests—United States, 23 August 2021–12 March 2022. *Morb. Mortal Wkly. Rep.* **2022**, *71*, 489–494. [CrossRef] [PubMed]
40. Usher, A.D. FIND documents dramatic reduction in COVID-19 testing. *Lancet Infect. Dis.* **2022**, *22*, 949. [CrossRef]

41. Flood, M.T.; Sharp, J.; Bruggink, J.; Cormier, M.; Gomes, B.; Oldani, I.; Zimmy, L.; Rose, J.B. Understanding the efficacy of wastewater surveillance for SARS-CoV-2 in two diverse communities. *PLoS ONE* **2023**, *18*, e0289343. [CrossRef]
42. Rabe, A.; Ravuri, S.; Burnor, E.; Steele, J.A.; Kantor, R.S.; Choi, S.; Forman, S.; Batjiaka, R.; Jain, S.; León, T.M.; et al. Correlation between wastewater and COVID-19 case incidence rates in major California sewersheds across three variant periods. *J. Water Health* **2023**, *21*, 1303–1317. [CrossRef]

IR
Reviewing IR Spectroscopy of Hydrocarbons

ICONS OF SPECTROSCOPY
Williams and Wright: The Legacy of the Coblentz Society

JANUARY 2025
VOLUME 40 | NO. 1

Spectroscopy®

SOLUTIONS FOR MATERIALS ANALYSIS

RAMAN

Identification of Dairy Products Using Raman Spectroscopy and Machine Learning

X-Ray

Micro X-Ray Fluorescence Spectroscopy in Food and Agricultural Products

ICP

Analyzing Production and Aging Effects in Lithium-Ion Batteries by LA-ICP-MS

Spectroscopy
AN MJH life sciences BRAND

485F US Highway One South, Suite 210
Iselin, NJ 08830 • (609) 716-7777

Editorial Advisory Board

Spectroscopy's Editorial Advisory Board is a group of distinguished individuals assembled to help the publication fulfill its editorial mission to promote the effective use of spectroscopic technology as a practical research and measurement tool. With recognized expertise in a wide range of technique and application areas, board members perform a range of functions, such as reviewing manuscripts, suggesting authors and topics for coverage, and providing the editor with general direction and feedback. We are indebted to these scientists for their contributions to the publication and to the spectroscopy community as a whole.

MANUSCRIPTS: To discuss possible article topics or obtain manuscript preparation guidelines, contact the managing editor at JChasse@mjhlifesciences.com. Publishers assume no responsibility for safety of artwork, photographs, or manuscripts. Every caution is taken to ensure accuracy, but publishers cannot accept responsibility for the information supplied herein or for any opinion expressed.

SUBSCRIPTIONS: For subscription information: *Spectroscopy*, P.O. Box 457, Cranbury, NJ 08512-0457; email mmhinfo@mmhgroup.com. Delivery of *Spectroscopy* outside the U.S. is 3–14 days after printing.

CHANGE OF ADDRESS: Send change of address to *Spectroscopy*, P.O. Box 457, Cranbury, NJ 08512-0457; provide old mailing label as well as =new address; include ZIP or postal code. Allow 4–6 weeks for change. Alternately, send change via e-mail to mmhinfo@mmhgroup.com for address changes or subscription renewal.

C.A.S.T. DATA AND LIST INFORMATION: Contact Stephanie Shaffer, (774) 249-1890; e-mail: SShaffer@mjhlifesciences.com

Reprints: Contact Stephanie Shaffer, e-mail: SShaffer@mjhlifesciences.com

INTERNATIONAL LICENSING: Contact Kim Scaffidi, e-mail: KScaffidi@mjhlifesciences.com

CUSTOMER INQUIRIES: Customer inquiries can be forwarded directly to MJH Life Sciences, Attn: Subscriptions, 2 Clarke Drive, Suite 100, Cranbury, NJ 08512; e-mail: mmhinfo@mmhgroup.com

Applications of Micro X-Ray Fluorescence Spectroscopy in Food and Agricultural Products

Derek D. Wright, Mark R. Zierden, Stephen Kolomyjec, and Benjamin Southwell

In recent years, advances in X-ray optics and detectors have enabled the commercialization of laboratory μXRF spectrometers with spot sizes of ~3 to 30 μm that are suitable for routine imaging of element localization, which was previously only available with scanning electron microscopy (SEM-EDS). This new technique opens a variety of new μXRF applications in the food and agricultural sciences, which have the potential to provide researchers with valuable data that can enhance food safety, improve product consistency, and refine our understanding of the mechanisms of elemental uptake and homeostasis in agricultural crops. This month's column takes a more detailed look at some of those application areas.

Food and agricultural products are important contributors to human health, and the elemental composition of these products is a critical determinant of plant yield, product quality, marketability, and nutritional value. Accurately analyzing the elemental composition of these products is essential for optimizing agricultural practices and ensuring the safety and quality of food products. X-ray fluorescence (XRF) spectroscopy is a powerful tool for elemental analysis in agricultural and plant sciences due to its ease of use and ability to provide quantitative or semi-quantitative analysis of solid materials. The non-destructive nature of XRF analysis allows the determination of elemental composition while preserving sample integrity including the analysis of live plants (1).

XRF spectroscopy is based on the ejection of an inner orbital electron by an incident X-ray, resulting in an electron hole that is subsequently filled by an electron from a higher energy orbital. This results in the fluorescent emission of element specific characteristic X-rays which can be detected by either an energy dispersive or wavelength dispersive spectrometer, yielding information on the elemental composition of the specimen. Significant advances in X-ray optics and detectors have facilitated the commercialization of laboratory micro XRF (μXRF) spectrometers (2). These instruments offer spot sizes in the ~3 to 30 μm range, enabling routine imaging of element localization within samples. Such non-destructive high-resolution elemental mapping could previously only be achieved on relatively small areas using scanning electron microscopy with energy dispersive spectroscopy (SEM-EDS), or by using μXRF beamlines at synchrotron facilities. The development of laboratory scale μXRF spectrometers allows for application across various research and industrial settings. The capability to collect data on element distribution from large and hydrated samples such as intact plants, with performance approaching that of synchrotron beamlines, opens a variety of new μXRF applications in food and agricultural sciences (3). These advancements offer a new tool to enhance agricultural productivity, food safety, and nutritional quality.

Micro-XRF spectroscopy can be utilized to ensure the quality of food products by detecting and quantifying both essential and trace elements. While bulk analysis techniques such as inductively coupled plasma mass spectrometry (ICP-MS), optical emission spectroscopy (ICP-OES), and conventional XRF analysis are well established, these techniques do not provide localized spatial information. This capability is crucial for verifying nutrient distribution and ensuring compliance

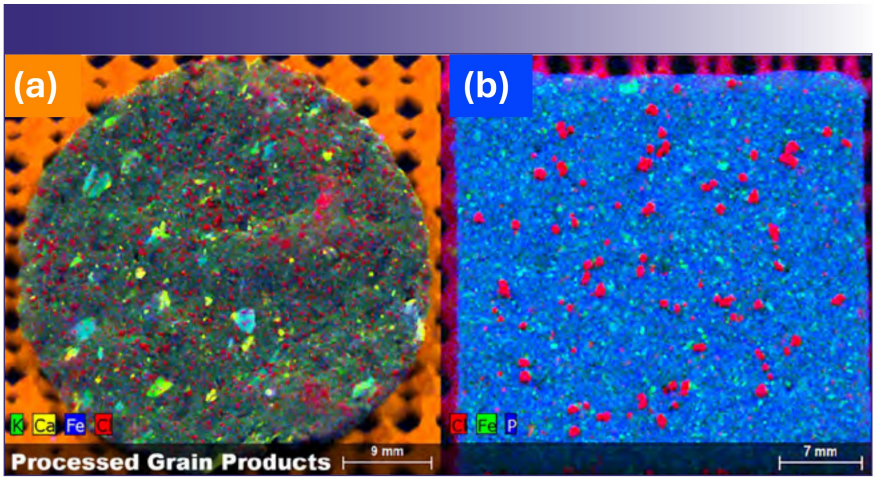

FIGURE 1: Processed grain products. Element maps of (a) tortilla chip, and (b) wheat cracker.

with regulatory standards. The accurate measurement of elements such as iron, calcium, and zinc in food products can help manufacturers ensure that products meet nutritional guidelines. This technique is also potentially useful in identifying specific sources of adulteration in food products, which is vital for maintaining the integrity of food supply chains and protecting consumer health (4). Adulteration can occur intentionally (such as the addition of cheaper ingredients to reduce costs or inorganic pigments to improve color), or unintentionally (through contamination during production or storage). The screening of food packaging materials for toxic elements such as lead or cadmium which may leach into food products can ensure the safety of packaging materials.

The imaging capability of µXRF allows for quantification or semi-quantification of element concentrations, but more importantly spatial localization which is useful for crop diagnostics (5). The ability to image the distribution of elements within live plant tissue provides new insights into the mechanisms of elemental uptake and homeostasis (6). This knowledge is essential for developing strategies to enhance nutrient efficiency and mitigate the accumulation of toxic elements in crops. Micro-XRF can reveal the localization of beneficial elements, such as calcium, which is important for preventing disorders like blossom-end rot or to detect potentially toxic elements, such as cadmium in vegetables (7). The objective of this work was to evaluate the efficacy of µXRF for elemental imaging in realistic samples and to demonstrate its performance in applications relevant to food and agricultural products.

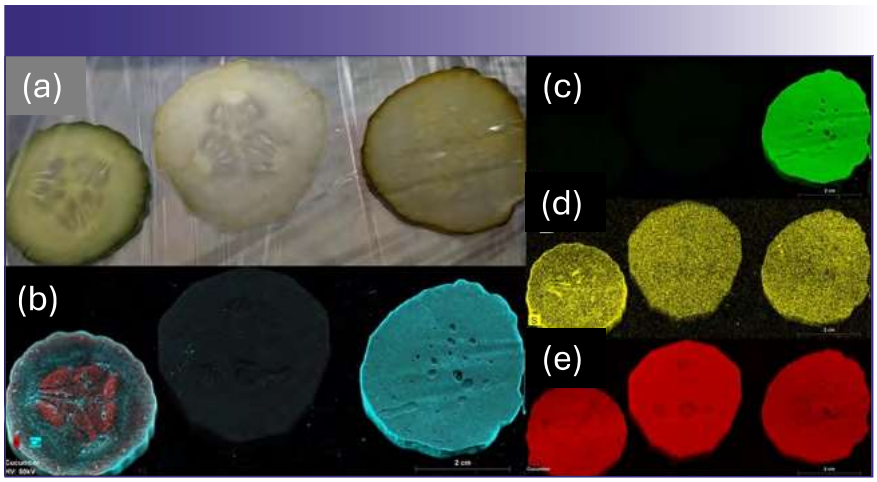

FIGURE 2: Three different treatments of cucumber fruit slices. (a) Visible light image of (from left to right) a freshly slice cucumber, a peeled & vinegared cucumber prepared for a salad, and a slice from a whole commercial pickle; (b) μXRF element distribution of potassium and calcium in the cucumber fruit slices from (a); (c) chlorine element map; (d) sulfur element map; (e) zinc element map.

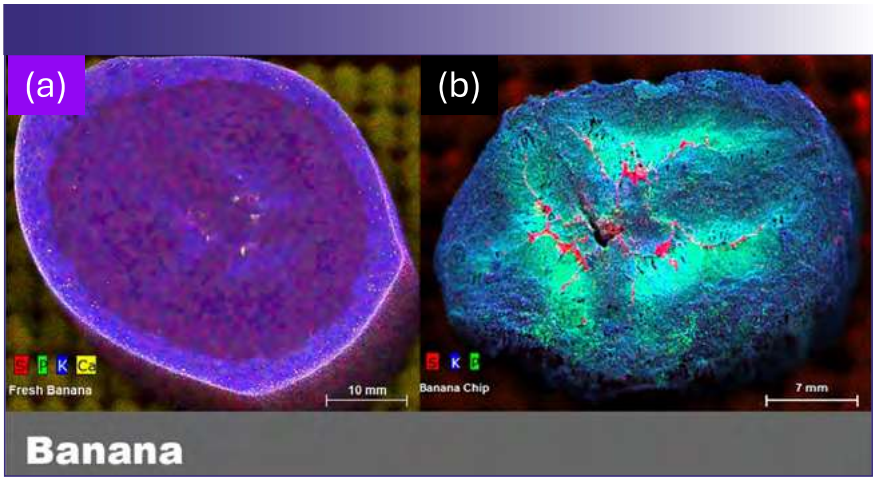

FIGURE 3: Bananas. Two μXRF images of banana slices. (a) Image shows nutrient distribution in a freshly sliced banana, while (b) the image on the right is a commercially prepared banana chip. Three primary nutrients are displayed in each (silicon, phosphorus, and potassium).

Experimental

Samples and Sample Preparation

Samples of food and plant materials were obtained from retail grocery outlets in Northern Michigan. Samples generally required no additional preparation steps for analysis except as follows: Samples were placed either directly on the sample stage with a layer of anti-slip material (foam shelf liner; tortilla chip, wheat cracker and applesauce cup), or placed on polyethylene terephthalate (PETE) film ("acetate film") supported on a 3D printed frame to reduce x-ray scattering from the stage (cucumbers, food packaging, and tomato leaf). The cucumber samples were secured to the acetate with low-density polyethylene (LDPE "cling wrap" prior to analysis to prevent drying. Tomato (*Solanum lycopersicum*) leaves were harvested from plants grown from seed in the Lake Superior State University (LSSU) greenhouse and were ~4 weeks old at the time of harvest. Evaporation during imaging was reduced by covering leaves in 3 μm mylar film (Fisher Scientific) and completed within ~2 hours of harvest. Other samples were imaged in air, and dry (vacuum stable) samples were imaged under vacuum (pressure = 2 mbar). Lead(II) chromate used for adulteration of cinnamon was purchased from Fisher Scientific.

Instrument Configuration

Elemental imaging by μXRF spectroscopy was conducted with an M4 Tornado Plus spectrometer (Bruker Nano GmbH). The spectrometer was equipped with a primary source consisting of a rhodium anode with polycapillary optics yielding an X-ray spot size of ~20 μm, and a second X-ray source consisting of a microfocus tungsten anode and variable collimator optics (0.5–4.5 mm). Fluorescence x-rays were detected using twin 60 mm^2 silicon drift detectors equipped with light element windows, enabling the detection of the carbon Kα peak at 0.277 keV when imaging under a vacuum or helium atmosphere. The stage accommodates samples weighing up to 7.5 kg and has a scan area of 16 x 19 cm (larger samples can be accommodated, so long as they don't collide with the interior housing during scanning). Peak identification, spectral deconvolution, and image processing was performed using the instrument software (M4 Esprit, Standard).

Results and Discussion

Food Quality Control and Effects of Processing on Nutrients

Consumer preference for nutritious food of uniform quality has resulted in food manufactures devoting significant attention to consistency of product aroma, flavor, texture, and appearance. For products where the elemental distribution affects product quality, μXRF offers unique advantages over conventional techniques for bulk analysis, as it offers insights on the element distribution of food components. One example where μXRF is particularly useful is imaging the distribution of salt within food products. Figure 1 shows the distribution of salt within a tortilla chip and a wheat cracker by mapping the Cl Kα (red). In the case of the wheat cracker, salt grains are relatively coarse and distributed at a relatively low density. The tortilla chip, by contrast, contains significantly smaller grains, distributed at a higher spatial density. Both the tortilla

chip and the wheat cracker also show distinct iron rich regions, with the tortilla chip also showing potassium/calcium rich regions (refer to Figure 1 for color codes). Given the nutritional importance of these elements, understanding the distribution and homogeneity of these elements may yield additional insights on the effects of food processing on nutrient distribution.

Additional examples of how μXRF can be utilized to understand the effects of food processing on nutrient distribution are illustrated in Figures 2 and 3. Figure 2 illustrates the differences in the elemental distribution resulting from the pickling process. In the fresh cucumber slice (Figure 2b), calcium is concentrated in the outer epidermal layers, along the vascular network, and in the ovule. Potassium, on the other hand, is abundant in the tissue immediately below the peel and is concentrated in the locular tissue surrounding the ovules. In both wet treatments, this localization is lost, however the calcium chloride found in pickling salts has clearly permeated the tissue in the pickled slice. The impacts of the calcium chloride is even more evident in the chlorine map (Figure 2c), where the element is virtually absent in the first two treatments. Figure 2d shows the sulfur distribution, while Figure 2e shows the zinc distribution. These two elements show the same delocalization of nutrients occurring during processing as indicated in Figure 2b (refer to Figure 2 for color codes).

Clear differences between a fresh banana and the commercial banana chip were observed (Figures 3a and 3b), particularly with regard to the silicon distribution. In the banana chip, the silicon distribution is concentrated in the central region, while silicon appears to be distributed more uniformly throughout the fresh banana slice. Possible explanations include alterations of the silicon distribution during the dehydration process or potentially the use of silica as a desiccant or anti clumping agent (no silica addition was indicated in the label ingredients). Additionally, it is also clear that calcium is enriched in the banana peel, which is typically discarded in common practice, relative to the fruit.

Food Adulteration

The presence of potentially toxic elements in food is an ongoing concern, whether introduced through natural processes or intentionally added. While some foods have long been recognized as a dietary source of elements sufficient to result in a public health risk (such as mercury in fish), in recent years a number of additional foods have been a source of concern. For example, in 2016 the U.S. Food and Drug Administration issued a risk analysis suggesting that exposure the arsenic from rice, a common ingredient in baby food, significant increased lifetime risk of bladder and lung cancers, and may constitute a public health concern (8). In addition to exposure from naturally occurring elemental impurities in foods, additional food safety risks may occur due to the intentional economic adulteration of foods. A recent example was the discovery of lead chromate in cinnamon, first identified in cinnamon applesauce in 2023 (9). The resulting investigation identified cinnamon containing lead concentrations as high as 5100 μg/g, and 1200 μg/g, of chromium,

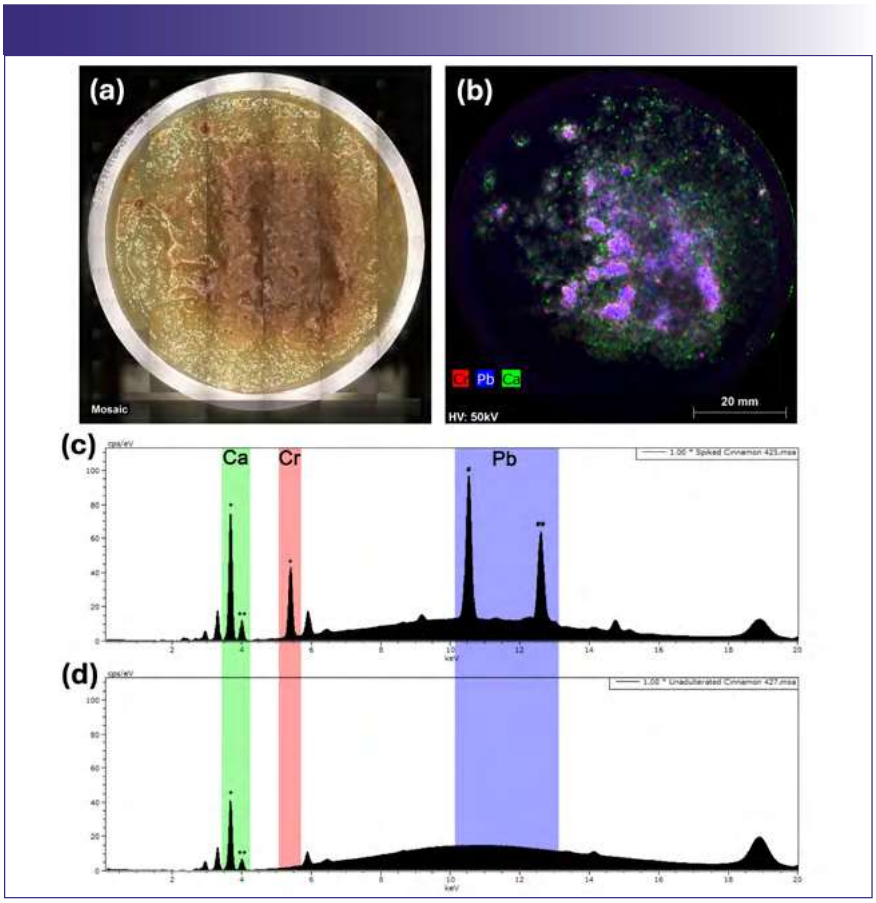

FIGURE 4: Adulteration of cinnamon in applesauce. Commercial ground cinnamon was purposely adulterated with 5000 µg/g lead(II) chromate. (a) Visible light image; (b) element map (Rh source) of Ca (green), Cr (red), and Pb (blue); (c) spectrum (Rh source) showing characteristic fluorescence peaks for Ca, Cr, and Pb (+ Kα, ++ Kβ, # Lα, ## Lβ); (d) spectrum (Rh source) of unadulterated cinnamon demonstrating that Cr and Pb are not detected.

and the recall of numerous cinnamon apple sauce products in March, 2024 (10).

As a demonstration of how µXRF might be used to detect adulteration in food products, commercial cinnamon was purposely adulterated with lead chromate (~5000 µg/g) and added to a commercial plain applesauce cup for elemental imaging (Figure 4). Lead (blue) and chromium (red) were readily detected in the adulterated applesauce and are clearly associated with the cinnamon. Calcium (green) was also highly enriched in the cinnamon relative to the applesauce, and the elemental images show that the lead chromate was not completely homogenous within the cinnamon despite vigorous manual mixing. Spot analysis on the cinnamon was subsequently performed using both the Rh source with polycapillary optics and the tungsten source with the 4.5 mm collimator (60 s live time, Figures 4c and 4d), and both spectra showed clear lead and chromium peaks with excellent signal to noise, confirming adequate sensitivity under both sets of analytical conditions.

While bulk analysis techniques such as ICP-MS and ICP-OES should have sufficient sensitivity to readily identify the lead and chromium contamination in this example, information on their spatial distribution would have been lost in the sample preparation/digestion process, potentially delaying the identification of the cinnamon as the adulterated component. Further, as µXRF imaging is non-destructive, the same sample could have been subsequently analyzed by additional techniques following imaging, whereas utilizing plasma spectroscopy techniques first would have precluded further spatially resolved analysis.

Identification of Elemental Components in Food Packaging

Food packaging is a necessary component of many commercial food items, and can provide significant benefits with respect to preservation of product quality as well as improving consumer appeal. Nonetheless, packaging components must be selected with care, as they have the potential to contribute to exposure to potentially toxic elements through various routes including migration into foods under certain conditions, hand to mouth transfer, and the potential of young children to chew on packaging materials (11). A particular risk is the potential use of inorganic pigments in packaging materials, especially in foods which may be consumed by children. While plasma spectroscopy techniques such as ICP-MS and ICP-OES are able to detect inorganic components such as pigments with high sensitivity, sample preparation and digestion is sometimes challenging for some packaging materials, and loss of spatial information may confound attempts to understand the source of contamination. For these applications, µXRF imaging proves to be advantageous.

Packaging materials for two food items (candy) that are likely to be consumed by children were analyzed by µXRF (Figures 5a–5d). The first item was a hard candy lollipop with a wax paper wrapper, and the second was a chocolate holiday candy with a foil wrapper. In both candies, the use of metal containing pigments was readily identified based on the correlation between metal distributions and the printed images. In both candies, vivid blue colors correlate to copper distribution, suggesting the use of copper based pigments. Similarly, white colors correlate with titanium distribution, suggesting the presence of titanium(IV) oxide (titanium white), a ubiquitous white pigment. In the case of the foil wrapper, aluminum was distributed uniformly throughout, consistent with an aluminum foil base as expected (refer to Figure 5 for color codes). Fortunately, neither sample was found to

CEM

BLADE™

The Future of Microwave Digestion

Learn more at cem.com/blade

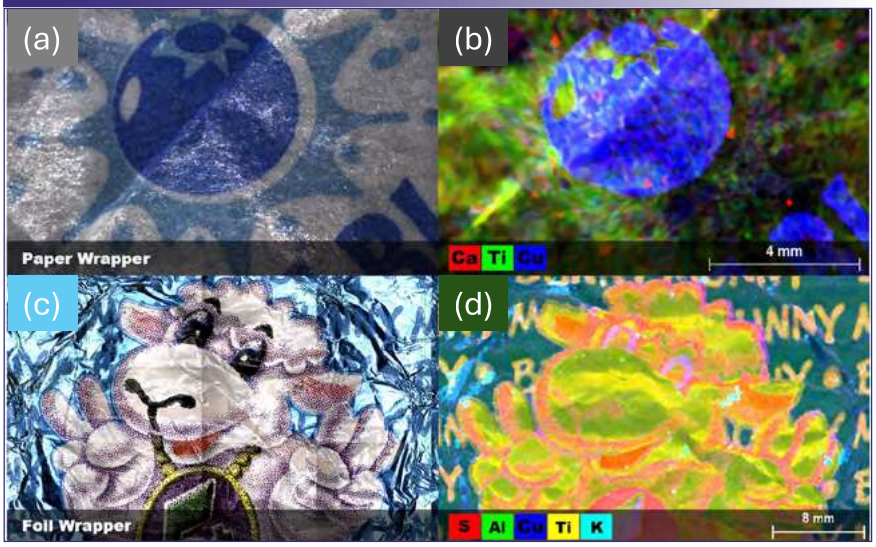

FIGURE 5: Candy wrappers. Elemental pigments and packaging material in food packaging. (a) Visible light image of a lollipop wrapper; (b) element map of the lollipop wrapper; (c) visible light image of a foil wrapper from a holiday chocolate candy; (d) Element map of the foil wrapper.

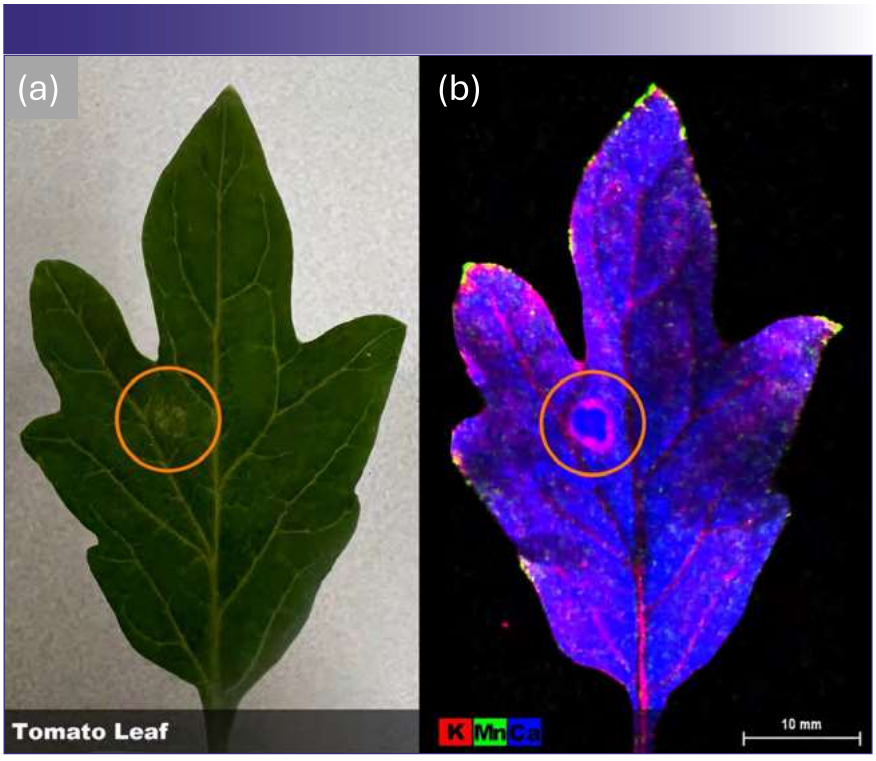

FIGURE 6: Intact tomato leaf. (a) A freshly picked leaf compared to (b) the μXRF image of the same leaf demonstrates the distribution of three major plant nutrients: potassium, manganese, and calcium. The μXRF image also clearly demonstrates the mobilization and redistribution of nutrients in response to damage (circled in both [a] & [b]).

contain pigments that might pose a high degree of risk such as lead chromate or cadmium yellow (cadmium [II] sulfide), but the relative ease of assigning elements with visual pigments makes μXRF imaging well suited to screening food packaging for potentially toxic elemental components, even in the case of the wax coated papers, which could prove challenging for other elemental imaging techniques such as scanning electron microscopy with energy dispersive X-ray spectroscopy (SEM-EDS).

Element Localization in Agricultural Plants

In conventional agricultural systems, crop yields are strongly affected by the availability of soil nutrient elements such as the macronutrients nitrogen, potassium, and phosphorus and various micronutrients such as calcium, iron, and manganese. Conversely, the presence of excess micronutrients or hazardous elements such as arsenic, lead, or cadmium may induce plant stress, reducing yields, and potentially rendering agricultural products unfit for consumption (12). Thus, a detailed understanding of the mechanisms that control elemental uptake and homeostasis is critical to maximizing crop yields and improving the sustainability of agricultural systems. Additionally, some plants show tolerance to elevated concentrations of potentially toxic elements and the ability to accumulate elevated concentrations, leading to growing interest in their application to phytoremediation of contaminated soils. From an economic perspective, identifying suitable species that efficiently accumulate elements of interest while still yielding usable biomass products or from which the elements can be recovered ("phytomining"), would significantly reduce the financial resources required to remediate contaminated sites. In each of these applications, the ability of μXRF imaging to provide information on the localization of elements within plant tissues can provide significant insights into the underlying mechanisms that affect element translocation and plant stress responses.

To investigate the distribution of key plant nutrient elements in juvenile tomato leaves, a freshly harvested leaf was analyzed by μXRF under atmospheric conditions (Figures 6a and 6b). Results showed that calcium (blue) was distributed throughout the leaf tissue, while potassium (red) was localized at higher concen-

trations within the veins. Conversely, manganese (green) was concentrated within the leaf tips and the margins. The leaf selected also contained a lesion (orange circle), with potassium concentrated at its margin, which suggests the involvement of potassium in plant response to tissue damage. Additionally, this data further demonstrates that caution must be used when using portable XRF instruments for in situ element monitoring, as the selection of analysis location may significantly impact results due to tissue localization.

Conclusion

The ability to perform high-resolution elemental imaging in the laboratory provides valuable data that can enhance food safety, improve product consistency, and deepen our understanding of elemental uptake and homeostasis in crops. By providing detailed insights into the elemental composition of food and agricultural products, µXRF supports efforts to enhance nutritional value, prevent contamination, and improve crop yields. As this emerging technology becomes more accessible to the fields of agricultural science, new and novel uses will continue to be developed. These applications will likely open currently unforeseen avenues of research and applications that improve the sustainability of agricultural systems.

Acknowledgments

Micro-XRF analysis was performed at the Micro Analysis and Spectroscopic Characterization (MASC) Lab at Lake Superior State University. The Bruker M4 Tornado Plus µXRF was acquired with funding from the National Science Foundation, NSF MRI Award #2320397.

References

(1) Feng, X.; Zhang, H.; Yu, P. X-Ray Fluorescence Application in Food, Feed, and Agricultural Science: A Critical Review. *Crit. Rev. Food Sci. Nutr.* **2021,** *61* (14), 2340–2350. DOI: 10.1080/10408398.2020.1776677

(2) Tsuji, K.; Matsuno, T.; Takimoto, et al .New Developments of X-Ray Fluorescence Imaging Techniques in Laboratory. *Spectrochim. Acta B: At. Spectrosc.* **2015,** *113,* 43–53. DOI: 10.1016/j.sab.2015.09.001

(3) Mijovilovich, A.; Morina, F.; Bokhari, S. N.; Wolff, T.; Küpper, H. Analysis of Trace Metal Distribution in Plants with Lab-Based Microscopic X-Ray Fluorescence Imaging. *Plant Methods* **2020,** *16,* 1–21. DOI: 10.1186/s13007-020-00621-5

(4) St. Jeor, V. L; Muroski, A. R.; McGuire, C.; Lape, A. Micro-X-Ray Fluorescence in Food Forensics. In *AIP Conference Proceedings* **2011,** *1365* (1), 411-414. American Institute of Physics. DOI: 10.1063/1.3625390

(5) Porfido, C.; Köpke, K.; Allegretta, I; et al. Combining Micro- and Portable-XRF as a Tool for Fast Identification of Virus Infections in Plants: The Case Study of ASa-Virus in *Fraxinus ornus L. Talanta* **2023,** *262,* 124680. DOI: 10.1016/j.talanta.2023.124680

(6) Ramos, I.; Pataco, I. M.; Mourinho, M. P.; et al. Elemental Mapping of Biofortified Wheat Grains Using Micro-X-Ray Fluorescence. *Spectrochim. Acta B: At. Spectrosc.* **2016,** *120,* 30–36. DOI: 10.1016/j.sab.2016.03.014

(7) Rizwan, M.; Ali, S.; Adrees, M., Ibrahim, M.; Tsang, D. C., Zia-ur-Rehman, M., ... & Ok, Y. S. A Critical Review on Effects, Tolerance Mechanisms and Management of Cadmium in Vegetables. *Chemosphere* **2017,** *182,* 90–105. DOI: 10.1016/j.chemosphere.2017.05.013

(8) U.S. Department of Health and Human Services, Food and Drug Administration, Center for Food Safety and Applied Nutrition. Arsenic in Rice and Rice Products Risk Assessment Report. May 13, 2014. revised March 2016.

(9) US FDA Investigation of Elevated Lead & Chromium Levels: Cinnamon Applesauce Pouches (November 2023) https://www.fda.gov/food/outbreaks-foodborne-illness/investigation-elevated-lead-chromium-levels-cinnamon-applesauce-pouches-november-2023 (accessed 2024-05-22)

(10) FDA Alert Concerning Certain Cinnamon Products Due to Presence of Elevated Levels of Lead. https://www.fda.gov/food/alerts-advisories-safety-information/fda-alert-concerning-certain-cinnamon-products-due-presence-elevated-levels-lead. (accessed 2024-05-22)

(11) Kim, K. C.; Park, Y. B.; Lee, M. J., Kim; J et al. Levels of Heavy Metals in Candy Packages and Candies Likely to be Consumed by Small Children. *Food Res. Int.* **2008,** *41* (4), 411–418.DOI: 10.1016/j.foodres.2008.01.004

(12) Martínez-Ballesta, M. C.; Dominguez-Perles, R.; Moreno, D. A.; et al. Minerals in Plant Food: Effect of Agricultural Practices and Role in Human Health: A Review. *Agron. Sustain. Dev.* **2010,** *30* (2), 295–309. DOI: 10.1051/agro/2009022

Derek Wright is a Professor of Environmental Science and is the Facility Coordinator of the Micro Analysis and Spectroscopic Characterization Laboratory at Lake Superior State University (Sault Ste. Marie, Michigan). He earned his PhD in 2008 from Rutgers University, and has expertise in both atomic and molecular spectroscopy, ICP-MS, XRF, SEM-EDS, and molecular techniques.

Mark Zierden is an Assistant Professor of Bioinorganic Chemistry at Lake Superior State University who specializes in plant uptake of elements and homeostasis. He earned his PhD in 2016 from Temple University and has expertise in both atomic spectroscopy and mass spectrometry.

Stephen Kolomyjec is an Associate Professor of Biology at Lake Superior State University who specializes in population genetics and imaging methods. He earned his PhD in 2011 from James Cook University and has expertise in genetic methods, molecular biology, zoology, electron microscopy, light microscopy, photography, and digital image analysis.

Benjamin Southwell is an Associate Professor of Bioanalytical Chemistry and is the Facility Coordinator of the Cannabis Center of Excellence at Lake Superior State University. He earned his MA in 2013 from Central Michigan University and has expertise in in both atomic and molecular spectroscopy, mass spectrometry, and molecular techniques.●